Summer 2023

Magmatic Evolution of the Chasca Orkho Lava Series and Its Magmatic Enclaves, Volcán Ollagüe, Central Andes

Nathaniel W. Lenhard
Missouri State University, nl5446s@MissouriState.edu

MAGMATIC EVOLUTION OF THE CHASCA ORKHO LAVA SERIES AND ITS MAGMATIC ENCLAVES, VOLCÁN OLLAGÜE, CENTRAL ANDES

A Master's Thesis

Presented to

The Graduate College of

Missouri State University

In Partial Fulfillment

Of the Requirements for the Degree

Master of Science, Geography and Geology

By

Nathaniel W. Lenhard

August 2023

MAGMATIC EVOLUTION OF THE CHASCA ORKHO LAVA SERIES AND ITS MAGMATIC ENCLAVES, VOLCÁN OLLAGÜE, CENTRAL ANDES

Geography, Geology, and Planning

Missouri State University, August 2023

Master of Science

Nathaniel W. Lenhard

ABSTRACT

Magma mixing is a common factor in the creation of intermediate composition magmas and a potential instigator of a volcanic eruption. Magmatic enclaves, physical evidence of magma mixing within a volcanic system, are a phenomenon whose mechanisms remain unclear and debated. Common hypotheses explaining the occurrence of magmatic enclaves within a host lava range from the repeated injection of a new magma into a shallow reservoir to the disruption of equilibrium within a stratified magma chamber. Within the Andean Central Volcanic Zone (CVZ), the occurrence of magmatic enclaves yields similar geochemical compositions to their respective host rocks, bringing more difficulty to the task of identifying magmatic end members before hybridization at these volcanic centers. In this study, whole rock and plagioclase feldspar phenocryst geochemical analysis is applied Volcán Ollagüe's Chasca Orkho lava series' magmatic enclaves and host lava to determine the magmatic evolution. This geochemical study utilizes major and trace element concentrations with electron probe microanalyzer (EPMA) and laser ablation ICP-MS on plagioclase feldspar phenocrysts and ICP-MS on whole rock samples from both magmatic enclave and host lava. Trace element data from plagioclase feldspar phenocrysts depict triangular mixing trends, evidence of three magmatic end members within the Chasca Orkho volcanic system: a primitive magma (38%-63% An), magma from a hybridized chamber (26% - 40% An), and a magma from an altered hybridized chamber (33%-55% An). Due to the petrologic textures and trace element mixing trends of the plagioclase feldspar phenocrysts, the magmatic evolution of the Chasca Orkho series is proposed to be evidence of a stratified magma chamber. The geochemical endmember originating from the hybridized reservoir is the first to be emplaced within the Chasca Orkho shallow reservoir, followed by the basaltic andesitic endmember from an isolated chamber, creating the stratified structure of the chamber. These two endmembers are the basis of the main mixing trend of the Chasca Orkho series. The third endmember is introduced to the hybridization reservoir and alters its composition, creating the muted third endmember of the Chasca Orkho series' magmatic evolution.

KEYWORDS: central andes, volcán ollagüe, volcanology, petrology, geochemistry, plagioclase feldspar

MAGMATIC EVOLUTION OF THE CHASCA ORKHO LAVA SERIES AND ITS MAGMATIC ENCLAVES, VOLCÁN OLLAGÜE, CENTRAL ANDES

By

Nathaniel W. Lenhard

A Master's Thesis
Submitted to the Graduate College
Of Missouri State University
In Partial Fulfillment of the Requirements
For the Degree of Master of Science, Geography and Geology

August 2023

Approved:

Dr. Gary Michelfelder, Ph.D., Thesis Committee Chair

Dr. Toby Dogwiler, Ph.D., Committee Member

Dr. Kevin Mickus, Ph.D., Committee Member

Julie Masterson, Ph.D., Dean of the Graduate College

ACKNOWLEDGEMENTS

I would like to thank the following people for their support during the course of my graduate studies. First and foremost, I would like to thank the National Science Foundation, the Geological Society of America, Missouri Space Grant Consortium, and Missouri State Graduate College for the funding of this this research and subsequent thesis. I would also like to thank Dr. Gary Michelfelder for this opportunity to study volcanology and geochemistry and the support that he has given me throughout this graduate program. I would like to thank both Dr. Toby Dogwiler and Dr. Kevin Mickus for being a part of my thesis committee as well. Special thanks go to Kenny Horkley of the University of Iowa and Dr. Barry Shaulis of the University of Arkansas for their instruction, input, and assistance with their Electron Microprobe and LA-ICP-MS instruments, respectively. Finally, I would like to thank my fellow graduate students César Bucheli, Sarah Rasor, and Bennett Van Horn for their support and solidarity during the course of this graduate program.

I would also like to thank several members of my family for their support during the course of my graduate studies. My wife, Kayleigh, has been incredibly supportive of me and my best friend during my time at Missouri State University. My parents, Matt and Jill Lenhard, have been consistently supportive and cheered me on throughout all of this. I would like to thank my grandfather Tom Nordtvedt, who instilled in me an appreciation of higher education since I was young. I would also like to thank my other grandfather, Harry Lenhard, who gave me my passion for geology.

I dedicate this thesis to my wife Kayleigh. Without her love and support for me, this master's program would have been nearly impossible to accomplish. With the completion of this thesis, we can begin to live the life we've always wanted to in our home state of Alaska.

TABLE OF CONTENTS

LIST OF TABLES

LIST OF FIGURES

INTRODUCTION

Magma mixing has been established as a common occurrence during magmatic evolution of volcanic systems as well as a precursor to volcanic eruptions and purported to be the origin of intermediate-composition magma bodies (Riehle et al., 1992; Feeley et al., 2008; Kent et al., 2010; Cooper & Kent, 2014; Kent, 2014; Jackson et al., 2018; Chen et al., 2020). While the process of constraining intermediate-composition magma formation in volcanic systems remains challenging, an approach based on petrologic observations and geochemical analysis can provide valuable insights into magmatic evolution of the system (White & Hofmann, 1982; Hildreth & Moorbath, 1988; Ginibre & Wörner, 2007; Feeley et al., 2008; Chadwick et al., 2012; Zhang et al., 2015; Taussi et al., 2019; Ubide et al., 2021a). Clear evidence of magma mixing can be physically observed in the form of xenoliths, magmatic enclaves, and disequilibrium textures within mineral phenocrysts while being corroborated through geochemical analysis (Feeley et al., 2008; Chadwick et al., 2012; Klemetti & Clynne, 2014; Zhang et al., 2015; Coote et al., 2018; Taussi et al., 2019; Barnes et al., 2021). Magmatic enclaves, quenched magma of a distinct composition in contrast to a 'host' lava, are subject to debate on where and when they form during the evolution of a volcanic system. While most studies agree that magmatic enclaves are formed from recharge into a shallow reservoir, triggering a subsequent eruption (Kent et al., 2010; Klemetti & Clynne, 2014; Taussi et al., 2019), some studies suggest that magmatic enclaves can also be related to compositionally stratified magma chambers before eruption (Riehle et al., 1992; Feeley et al., 2008). The introduction of new data for magmatic evolution and magma mixing conditions for volcanic centers can provide better insights into magma storage within the crust.

The western margin of the South American continent is a hub of historical and contemporary volcanism within a subduction setting. One of three regions of volcanism along the continent, the Central Volcanic Zone (CVZ) of the Central Andes displays periodic eruptions within several volcanic provinces (Gregory-Wodzicki, 2000). Of these volcanic provinces, the Altiplano-Puna Volcanic Complex (APVC), straddles the border between northern Chile and Bolivia, with many of its eruptive centers utilized as boundary markers between the two countries. In addition, the APVC is underlain by a large low-velocity seismic zone, inferred to be a voluminous magma reservoir known as the Altiplano-Puna Magma Body (APMB) that influences recent and contemporary volcanism in the province (Chmielowski et al., 1999; Gregory-Wodzicki, 2000; Ward et al., 2014; Perkins et al., 2016; Pritchard et al., 2018). The presence of the APMB and other large magma reservoirs in addition to thick Andean crust and subduction processes creates a complex setting for volcanism within the Altiplano-Puna Volcanic Complex and the greater Andean Central Volcanic Zone (Hildreth & Moorbath, 1988; Gregory-Wodzicki, 2000; Rosenbaum et al., 2021). One example of a volcanic center within this complex setting is Volcán Ollagüe, a composite stratovolcano utilized as a boundary peak on the border of Chile and Bolivia (Feeley et al., 1993; Tibaldi et al., 2006; Vezzoli et al., 2008; Michelfelder et al., 2013). Volcán Ollagüe is located at the northwest edge of the APMB low-velocity zone and shows evidence of magma mixing in the form of magmatic enclaves scattered throughout its lava flows (Feeley et al., 1993; Feeley & Davidson, 1994; Feeley & Sharp, 1995). While previous studies have focused on Central Andean volcanism and Volcán Ollagüe, these studies have utilized whole-rock geochemical analysis, which only provides a general picture of magmatic evolution, especially when intermediate composition magmas have extensively hybridized (Hildreth & Moorbath, 1988; Ginibre & Wörner, 2007; Font et al., 2008; Ginibre &

Davidson, 2014; Rosenbaum et al., 2021). In response, micro-analysis of geochemistry within phenocrysts such as plagioclase feldspar can record slight variations in composition and conditions within a system, providing an excellent alternative to whole-rock geochemistry while studying magmatic evolution in volcanic systems (Tepley et al., 1999; Davidson et al., 2004, 2007a, b; Ginibre & Wörner, 2007; Font et al., 2008; Ginibre & Davidson, 2014; Klemetti & Clynne, 2014; Barnes et al., 2021; Chew et al., 2021; Lormand et al., 2021; Ubide, 2021b).

Volcán Ollagüe's unique position on the northwest boundary of the APVC and underlying APMB in addition to the clear evidence of magma mixing within its erupted material makes it a prime candidate for geochemical micro-analysis to better understand the magmatic evolution of the volcanic center. The presence of magmatic inclusions, most heavily concentrated in the Chasca Orkho lava series raises several questions: 1) Do the magmatic inclusions present in the Chasca Orkho series represent xenoliths or enclaves; 2) What component of the Chasca Orkho series do these inclusions represent; and 3) Are these magmatic enclaves from the Chasca Orkho series representative of a stratified magma chamber? This study will test the hypothesis that the presence of enclave-rich magmas during the eruption of the Chasca Orkho series represents recharge events into a shallow reservoir that is not compositionally stratified. To test this hypothesis, this study will be divided into two distinct parts of whole-rock geochemical analysis and geochemical micro-analysis of plagioclase feldspar within each of our whole-rock samples. This study of the magmatic evolution of the Chasca Orkho series' host lava and magmatic enclaves, specifically the micro-analysis of plagioclase feldspar phenocrysts, will provide in greater detail a snapshot of the conditions and factors influencing Volcán Ollagüe's plumbing system. Whole rock trace element chemistry, mineral and petrologic textures, mineral major element chemistry, and mineral trace element

chemistry will be combined with previous whole rock data from Feeley & Davidson (1994) to recreate the magmatic evolution of the Chasca Orkho lava series.

GEOLOGIC BACKGROUND

Andean Central Volcanic Zone

Along the subduction margin of the South American continent, the Central Andes contains both a record of significant magmatism and contemporary magmatism within the Andean Central Volcanic Zone (CVZ; Salisbury et al., 2011; Michelfelder et al., 2013). Evidence of large volcanic events in the CVZ is evident with the occurrence of the Altiplano-Puna Volcanic Complex (APVC), a series of ignimbrite bodies dating from 1 Ma to 11 Ma with links to a voluminous magma reservoir known as the Altiplano-Puna Magma Body (APMB; de Silva, 1989; Salisbury et al., 2011; Michelfelder et al., 2013; Pritchard et al., 2018). Above the northern boundary of the APMB, Volcán Ollagüe (21º17'S, 68º11'W) and nearby parasitic and dacitic domes are located approximately 200 km northeast of the city of Calema along the Boliva-Chile border (Fig. 1; Ward et al., 2014). The volcanic center is constructed upon the 5 Ma to 8 Ma Carcote and Chuhuilla Ignimbrites of the APVC in the Western Cordillera of the Central Andes (Tibaldi et al., 2006; Salisbury et al., 2011; Michelfelder et al., 2013).

Volcán Ollagüe

Volcán Ollagüe's eruptive history spans from approximately 1.2 m.y, with the last major eruptive phase ending at 130 ka (Fig. 2; Feeley & Davidson, 1994; Feeley & Hacker, 1995; Tibaldi et al., 2006; Vezzoli et al., 2008; Michelfelder et al., 2013). Volcán Ollagüe is consolidated into four major eruptive phases: the Vinta Loma, Santa Rosa, El Azufre, and Santa Cecilia lava series (Tibaldi et al., 2006; Vezzoli et al., 2008 Michelfelder et al., 2013). The oldest eruptive series, named the Vinta Loma series, is primarily exposed in the northeastern section of

the volcanic center and is andesitic to dacitic in composition and has a thickness of 20 – 90 m depending on location (Feeley et al., 1993). The Vinta Loma series contains plagioclase, ortho- and clinopyroxene, amphibole, and trace amounts of biotite (Feeley et al., 1993). Overlying the Vinta Loma, the Santa Rosa series has a compositional range of basaltic andesitic to dacitic and contains pyroclastic deposits, lava flows, and scoria deposits primarily exposed on the southeast area of the volcanic center (Fig. 2; Vezzoli et al., 2008). The El Azufre series is exposed in the southeast section of Volcán Ollagüe, overlying the Santa Rosa series situated in the area, as well as being observed around the summit (Fig. 2; Vezzoli et al., 2008). Lava flows from the El Azufre series can reach up to 200 m thick, interpreted as a former lava lake, and includes andesitic lava flows (Vezzoli et al., 2008). The youngest lava series erupted at Volcán Ollagüe is the Santa Cecilia series, a combination of lava domes trending SE to NW and lava flows exposed on the southwestern flank of the volcanic center (Fig. 2; Vezzoli et al., 2008). In addition to these major lava series, a notable part of the upper Santa Rosa and lower El Azufre series is the Chasca Orkho lava series, primarily noted as flank eruptions to the southeast and not originating from the main vent (Fig. 2; Tibaldi et al., 2006; Vezzoli et al., 2008). Typically, large concentrations of plagioclase, biotite, amphibole, lesser amounts of ortho- and clinopyroxene, and instances of olivine are present in Chasca Orkho hand samples (Feeley et al., 1993; Feeley & Davidson 1994). Within the beginning of the El Azufre series, the Chasca Orkho parasitic dome erupted and produced the samples that are used in this study (Vezzoli et al., 2008).

The Chasca Orkho parasitic domes are basaltic andesitic to dacitic in composition and contain magmatic enclaves that range from basaltic andesitic to andesitic (Feeley et al., 1993; Michelfelder et al., 2013). The magmatic enclaves of the Chasca Orkho series are notable; while most lava series at Ollagüe contain trace amounts of enclaves 1 cm or less in diameter, the

Chasca Orkho series contains enclaves up to 15 cm in diameter in greater proportion to its counterparts (Feeley et al., 1993; Michelfelder et al., 2013). The presence of magmatic enclaves within erupted material has been stated as evidence for extensive magma mixing and recharge within a magmatic system (Feeley et al., 2008; Kent et al., 2010; Kent, 2013; Cooper & Kent, 2014). Therefore, the presence of magmatic enclaves within Volcán Ollagüe's Chasca Orkho lavas indicate that a significant degree of mixing and recharge occurred prior to eruption. This in turn supports the perspective that Ollagüe has experienced and represents a significant degree of interaction with the Andean crust, APMB, and subduction-related magma bodies.

METHODS

For this study, 12 polished thin sections and 28 whole rock samples from the Chasca Orkho lava series were used to determine the petrology, major element, and trace element concentrations for both whole rock and plagioclase phenocryst samples. Plagioclase phenocrysts were subjected to major and trace element analysis while bulk-rock samples underwent trace element analysis. A list of all samples used for this study can be found in Table 1.

Whole rock geochemistry

A total of 28 whole rock samples, 18 host lava and 10 enclave samples collected by Feeley et al. (1993) were analyzed by inductively coupled plasma mass spectrometry (ICP-MS) for trace element concentrations (Sc, Cu, Zn, Rb, Sr, Y, Zr, Nb, Cs, Ba, La, Ce, Pr, Nd, Sm, Eu, Gd, Tb, Dy, Ho, Er, Tm, Yb, Lu, Hf, Ta, Pb, Th, U). Major element compositions for these samples were determined by Feeley & Davidson (1994). Whole rock samples selected for this analysis were crushed and powdered before beginning acid digestion. For each sample, 50mg of powder was measured into Teflon beakers and introduced to a 5 mL, 1:1 ratio of distilled HF and HNO_3 before sitting for approximately 12 hours and being heated to approximately 100°C for evaporation. The samples were then introduced to 4 mL of distilled HNO_3 and HCl for a similar temperature and period of time before evaporation. The final round of acid digestion consisted of 3 mL of distilled HNO_3 introduced to each sample before being diluted to a 3% HNO_3 solution after a further 12 hours of digestion. Our digested whole rock samples were then placed in labeled sample beakers for subsequent ICP-MS analysis. This analysis occurred at Missouri State University using an Agilent 7900 Quadrupole ICP-MS. Our whole rock samples were measured against USGS

reference materials BCR-2, STM-2, and RGM-2. A summary of all whole rock sample and standard trace element concentrations can be found in Table 1.

Electron probe micro-analysis

Major element concentrations of plagioclase feldspar phenocrysts were analyzed using polished thin sections of four host lava samples and eight enclave samples using electron probe microanalysis (EPMA). We conducted this analysis at the University of Iowa's Iowa Advanced Technology Laboratory (IATL) using a the JEOL JXA-8230 Superprobe instrument situated there. For each thin section sample, between 15-25 plagioclase phenocrysts were selected for this analysis. Backscatter electron (BSE) imaging and chemical maps were collected for select plagioclase feldspar samples as well as each thin section. For each mineral sample, three to five spots were analyzed to represent the core, mantle, and rim of the crystal. A subset of selected plagioclase samples, up to five per thin section, were subject to spot transects from core to rim, resulting in 15-41 spot analyses depending on the size of the phenocryst in question. Plagioclase phenocrysts from all samples were analyzed using an accelerated voltage of 15kV, emission current of 20 nA, and a working distance of 11.1 mm. Reference materials for plagioclase phenocryst analysis include Astimex Plagioclase, Cr-Pyrope and Orthoclase as well as in-house University of Iowa (UI) Albite and Anorthite reference materials.

Laser ablation ICP-MS

A subset of plagioclase feldspar phenocrysts from each sample was selected for trace element analysis by Laser Ablation Inductively Coupled – Mass Spectrometry (LA-ICP-MS Three sets of corresponding host lava and magmatic enclave samples (OlA-90-15/15i, OLA-90-21/21iA, OLA-90-26/26i) analyzed for major element concentrations using EPMA techniques were selected

for analysis. From each sample, 15-20 plagioclase feldspar phenocrysts were analyzed using a combination of core to rim transects and spot analyses. Each spot and transect analysis determined the concentrations of Li, Mg, Si, Sc, Ti, Cr, Fe, Zn, Rb, Sr, Y, Zr, Nb, Cs, Ba, La, Ce, Pr, Nd, Sm, Eu, Gd, Tb, Dy, Ho, Er, Tm, Yb, Lu, Hf, Pb, Th, and U. For each analysis, any fractures, melt inclusions, secondary growths and sieving textures were avoided when observed in plagioclase samples. All selected plagioclase feldspar phenocrysts were subject to 3-5 spot analyses from core to rim with a spot size of 50 μm, a 10 Hz rate, shock count of 200, and a power level of 3 J/cm^2. In each host lava and enclave sample, at least five plagioclase phenocrysts were also subjected to a core to rim transect analysis with identical settings and a speed of 10 μm/s. These phenocrysts are the same ones selected for spot transect analysis during microprobe analysis. A groundmass spot analysis was completed immediately adjacent to 1-4 phenocrysts in each host lava and enclave sample in order to characterize trace element characteristics of the final liquid during eruption. Internal standards for our laser ablation analysis were reference materials NIST610 and NIST612 (Jochum et al., 2011). Precision of all elements for reference material NIST 610 was under 5% with two standard deviations. Precision of most NIST 612 element concentrations was under 5% with two standard deviations, with the exception of elements Ti (6.3%), Fe (36.6%), Zn (5.5%), and Zr (49.8%). Trace element concentration results were reduced using Iolite methodology from Woodhead et al. (2007) and Paton et al. (2011).

RESULTS

Whole Rock Geochemistry

Trace Element Data

Whole rock major element data used in this study was collected by Feeley & Davidson (1994). The results of this whole rock data are fully described in Feeley & Davidson (1994). Whole rock major and trace element data is presented in Table 1 and illustrated in Figures 3-5**.** Select trace element concentrations plotted against FeO wt% (Feeley & Davidson, 1994) show linear trends in magma composition (Fig. 3). Major element data from Feeley & Davidson (1994) corresponded with trace element chemistry data collected for this study, Sr/Y ratios were plotted against SiO_2 wt% to observe compatibility with the deeper, stable-garnet regions of the Andean crust, with host lava samples ranging from 22.8 – 35.3 (Fig. 4). Generally, a flat linear trend is observed within both host lava and enclave whole rock sample populations. Trace element concentrations of whole rock host lava samples were normalized by chondrite values from McDonough & Sun, (1995) within Figure 5. Chondrite-normalized La/Yb [$(La/Yb)_N$] and Eu/Eu* ratios for host lava whole rock samples range from 14.28 – 42.92 and 0.74 – 0.87, respectively (Figs. 4-5). Likewise, $(La/Yb)_N$ and Eu/Eu* ratios for magmatic enclave whole rock samples range from 11.12 – 19.69 and 0.78 – 1.71, respectively (Fig. 4).

Whole rock trace element concentrations of both host lava and magmatic enclaves are extensively overlapped. Whole rock samples of magmatic enclaves contain concentrations of Rb from 13.1 – 62.4 ppm, Sr from 189 – 394 ppm, Y from 6.19 – 10.9 ppm, Ba from 281 – 831 ppm, Nd from 7.33 – 17.5 ppm, and Th from 1.85 – 3.17 ppm (Fig. 4). Linear trends are observed for Rb/Sr and Eu/Eu* (0.37 – 0.78 and 0.73 – 0.86, respectively) while ratios of

Sm/Yb, $(La/Yb)_N$, and Nb/Zr are represented by positive trends (3.6 – 8.5, 12.57 – 42.65, 0.07 – 0.19, respectively; Fig. 4). Additionally, Sr/Y ratios plotted against SiO_2 wt% content for whole rock enclave samples continue the flat, linear trend of the host lava samples (Fig. 4). Magmatic enclave samples contain higher FeO wt% values than their host lava counterparts and generally continue the same trends as their host lava counterparts (Figs 3-4).

Mineral Geochemistry

Host Lava Petrology

Polished thin section samples OLA-90-15, 20, 21, and 26 are derived from the El Azufre eruptive series, specifically the Chasca Orkho lava flows (Figs. 6-8). These samples show common similarities, with textures being generally porphyritic and average mineral assemblage of plagioclase > hornblende > biotite. Glomerocrysts (>> 1%) can be found within samples OLA-90-20 and 26. Plagioclase feldspar within these samples generally show oscillatory zonation with smaller populations of weak zoning with some phenocrysts exhibiting no zonation except for at the rims. Disequilibrium textures including resorbance and sieving are observed on approximately select analyzed plagioclase feldspars. When observed, these disequilibrium textures appear on the rims and occasionally the mantles of plagioclase feldspar.

Magmatic Enclave Petrology

Polished thin sections OLA-90-15i, 20i, 21iA, 26i, and 44iA-D are magmatic inclusions corresponding to host rock samples described above. Three textures are found within this spread of samples: OLA-90-15i and 21iA have a diktytaxitic texture (Fig. 3-4) while inclusions OLA-90-20i and 26i show a combination of chilled margin and porphyritic textures (Fig. 5). The average mineral assemblage within these magmatic enclave samples is plagioclase > hornblende > biotite > pyroxene. Within the diktytaxitic and chilled margin textures, plagioclase feldspar are

distinctly smaller than those in porphyritic textured samples. Additionally, plagioclase within these textures mainly show no distinct zonation with the exception of a thin, lighter rim (Fig. 6). When a porphyritic texture is observed within an enclave sample (e.g., OLA-90-20i and 26i) plagioclase feldspar show oscillatory zonation (Fig. 7). When larger plagioclase feldspar grains are observed within the diktytaxitic and chilled margin textures, they show extensive disequilibrium textures from core to rim. In all enclave samples, disequilibrium textures are observed mainly within the mantles of plagioclase feldspar grains (Fig. 8).

Plagioclase Feldspar Major Element Data

Plagioclase major element data for both host rock and magmatic enclave samples are represented in Table 2**,** illustrated in Figures 9-10, and fully summarized in Appendix A. Calculated molar percentage of Anorthite in plagioclase samples (Molar An %) for all analyzed plagioclase phenocrysts range from 26.2% - 68.3%. On average, plagioclase from sample OLA-90-15 have the lowest molar An % contents ranging from 26.2% - 39.1%, while plagioclase from sample OLA-90-15i had the highest range of molar An % concentrations ranging from 38.9% - 61.9% (Fig. 9). However, sample OLA-90-21iA contains core, mantle, and rim analyses that have both higher and lower SiO_2 contents compared to the vast majority of other points. FeO wt% content is contained between 1.4% - 0.1% and 0.1% - 1.9% for host lava and magmatic enclave samples, respectively. MgO wt% is ranged between 0% - 0.17% and 0% - 0.2% for host lava and magmatic enclave samples, respectively, and TiO_2 wt% ranges from 0% - 0.2% in both host lava and magmatic enclave samples. Linear trends show definitive mixing trends between different samples, while negative concave trends are seen in Figure 10**.** FeO, MgO, and TiO_2 wt% contents for plagioclase phenocrysts were calculated and plotted against Molar % Anorthite (An) content (Fig. 10). FeO and MgO when plotted against An % are slightly concave while

TiO_2 plotted against An % is very nebulous; most likely due to the very low wt% of TiO_2 in plagioclase (Fig. 10).

Plagioclase Feldspar Trace Element Data

A comprehensive list of trace element concentrations in plagioclase phenocrysts is summarized in Table 3 and is represented in Figures 5 and 11. Trace element data from analyzed plagioclase phenocrysts was analyzed using laser ablation ICP-MS and can be utilized to categorize different magma sources as well as detailed indicators of magma chamber processes. Overall, trace elements Sr and Ba are focused on because they can replace Ca as the primary cation in plagioclase feldspar's chemical structure. For all analyzed plagioclase samples in both host lava and inclusion sample plagioclase phenocrysts, Sr ranges from 858 ppm to 2985 ppm with an average 1536 ppm. Within host lava sample plagioclase phenocrysts, Sr has a range of 858 ppm – 2985 ppm with an average of 1580 ppm. For inclusion sample plagioclase phenocrysts, Sr has a narrower range of 1036 ppm – 2015 ppm and an average of 1484 ppm. While the ranges of Sr concentration within host lava and enclave samples is significantly different, the averages of the two sample types remains remarkably similar, with a relatively small difference of 104 ppm. For plagioclase phenocrysts within all samples, the concentration of Ba ranges from 3.76 ppm to 1563 ppm with an overall average of 514 ppm. Plagioclase phenocrysts analyzed in host lava samples range in Ba from 130 ppm – 1563 ppm along with an average of 614 ppm. Inclusion plagioclase phenocrysts yield a range of 3.76 ppm – 972 ppm and an average of 393 ppm. Core-to-rim transect analyses for Mg, Fe, Sr, and Ba content show slight changes in magmatic composition (Figs. 6-8, 11). Generally, core-to-rim transect trends of Mg and Fe content mimic each other from the core to rim of any analyzed plagioclase phenocryst, but in some cases large spikes in Mg concentration are observed without any corresponding

spike in Fe concentration, which may point of the introduction of a magma body with a unique trace element signature. These anomalous spikes in Mg concentrations are typically best observed in the mantles or rims of host lava and enclave plagioclase phenocrysts, indicating that this potential magma introduction occurred later in the evolution of the Chasca Orkho series. Likewise, trends of Sr and Ba largely follow each other with Ba concentrations observably more extreme compared changes within Sr concentrations. It should also be noted that when a spike of both Mg and Fe concentrations is observed, a corresponding decrease in both Sr and Ba concentrations is also observed (Figs. 6-8, 11).

Plagioclase phenocrysts analyzed from OLA-90-15 show Sr and Ba content trends with oscillatory zoning and either little to no change in overall concentration or a gradual increase in concentration from core-to-rim. The corresponding inclusion sample OLA-90-15i, Sr and Ba trends show overall concentrations staying largely the same from core-to-rim, with instances of gradual increases and decreases. This corresponds with the zonation of plagioclase phenocrysts from OLA-90-15i; while samples from OLA-90-15 typically have more oscillatory zonation, plagioclase from its reciprocal enclave sample are largely observed to have very few zones and a distinct rim zonation.

Plagioclase phenocrysts from samples OLA-90-21 and OLA-90-21iA show Sr and Ba concentrations and trends that are relatively similar. The majority of these plagioclase phenocrysts have similar zoning profiles with Sr and Ba contents generally staying the same throughout the core-to-rim transects. This suggests that this host lava and magmatic enclave sample pair represents magma bodies that have experienced a similar magmatic evolution, undergone a significant degree of mixing, or a combination of the two. Such similarities

therefore provide evidence that the shallow reservoir of Volcán Ollagüe may have been at least partially stratified.

Plagioclase phenocrysts in sample OLA-90-26 contain Sr and Ba content trends that mirror each other in gradual positive linear trends (OLA-90-26-06; Fig. 8). In other transected phenocrysts, several distinct peaks of Sr and Ba concentration increase, corresponding with a sharp increase in Fe and Mg concentration in the same section of the phenocryst (Fig. 8). These large concentrations of Fe and Mg with corresponding variability in Sr and Ba concentrations can once again be interpreted as potential recharge events between the shallow reservoir of Ollagüe and a deeper source. With sample OLA-90-26i, plagioclase phenocrysts show similar trends with Mg and Fe as well as Sr and Ba concentrations; split between linear trends with relatively little variability and linear trends with large spikes in concentrations (Fig. 8).

Elements Li, Sr, Rb, La, Ba, Nd, and Nb were plotted against Fe concentrations to aid in the interpretation of each host lava and enclave sample's magmatic history. Iron was chosen for other trace elements to be plotted against because 1) Fe concentration in plagioclase phenocrysts changes with small alterations within magmatic compositions, and 2) Fe is a minor element within plagioclase feldspar chemical structure. Elements Rb, Sr, Y, Ba, Nd, and Th were chosen to be plotted against Fe because they are representative of all elements analyzed using LA-ICP-MS and can be compared against whole rock trace element concentrations. Rubidium and Nd plots have positive, generally concave trends with the majority of analyzed spots with low (< 30 ppm) concentrations (Fig. 11). Plagioclase from samples OLA-90-15, OLA-90-21, and OLA-90-21iA have the highest overall concentrations of these elements. Barium shows steeper linear trends with increasing Fe content (Fig. 11). Barium concentration ranges from 130 – 1562 ppm for almost all analyzed spots, but several mantle and rim analyses of plagioclase from sample

OLA-90-15i are recorded as below 20 ppm (Fig. 11). Within Figure 11, a triangular mixing trend is observed. Within this triangular trend, plagioclase from samples OLA-90-15 and OLA-90-15i form a positive linear slope, samples OLA-90-21, OLA-90-21iA, OLA-90-26, and OLA-90-26i composing a flat, linear trend, and mantle analyses of samples OLA-90-15 and OLA-90-21 composing a weak, linear, negative slope. For all elements plotted against Fe with the exception of Sr, plagioclase phenocrysts from sample OLA-90-15i have the lowest concentrations overall (Fig. 11). Likewise, plagioclase phenocrysts from sample OLA-90-15 generally have the highest overall concentrations in Figure 11. Additionally, corresponding samples OLA-90-21 and OLA-90-21iA as well as OLA-90-26 and OLA-90-26i show plagioclase phenocrysts with highly similar trace element concentrations, especially for trace elements with high abundance in plagioclase feldspar (Fig. 11). These observations are largely concurrent with those of major element composition data (Fig. 9).

DISCUSSION

Plagioclase feldspar is a common mineral phase throughout a large range of magma compositions and settings and is able to potentially record events such as magma mixing and differentiation with little to no diffusion occurring between the cores, mantles, and rims of an individual crystal (Tepley et al., 1999, 2000; Davidson et al., 2007a, 2007b; Shane et al., 2019; Chen et al., 2020). Therefore, the magmatic evolution of the Chasca Orkho host lava and magmatic enclaves can be understood through the analysis of plagioclase feldspar phenocryst petrology and chemistry within each host lava or enclave sample. Here, we present our interpretations and model of the magmatic evolution of the Chasca Orkho lava series and its shallow reservoir prior to eruption.

Whole Rock Interpretations

Whole rock trace element data trends and populations from both the Chasca Orkho series and Volcán Ollagüe reveal interesting interpretations. The separation between our trace element data trends and data described by Feeley & Davidson (1994) infers that the magmatic systems of Volcán Ollagüe and the Chasca Orkho parasitic domes are separate entities (Fig. 3). If there were a shared system or reservoir between these populations, there would be notable interaction between the two datasets (Fig. 3). Therefore, we can establish that the Chasca Orkho parasitic domes have their own distinct magmatic system and reservoirs separate from Volcán Ollagüe.

Flat linear trends of the whole rock trace element ratios suggest Chasca Orkho lavas have experienced differentiation as time progresses (Fig. 4). The utilization of whole rock geochemistry allows for contextualization with similar studies. Whole rock geochemical studies

observing the larger scope of volcanism within the Central Andes have established modeled geochemical endmembers, specifically Blum-Oeste & Wörner, (2016). These modeled endmembers consist of a rhyodacitic, a basaltic andesitic, and an enriched basalt endmember (Fig. 4; Blum-Oeste & Wörner, 2016). When imposing the geochemical endmembers of the region described by Blum-Oeste & Wörner, (2016), our whole rock data from the Chasca Orkho series can be seen to plot in between the rhyodacitic and basaltic andesitic endmembers, specifically within plots of Sr/Y, $(La/Yb)_N$, and Sm/Yb (Fig. 4). As a result, we can infer that both the Chasca Orkho lava series and Volcán Ollagüe have major influences from sources that best represent two of three described magmatic endmembers within the Andean Central Volcanic Zone (Fig. 4; Blum-Oeste & Wörner, 2016).

Petrology and Mineral Origins

To understand the differences between the magmatic inclusions and host lava of the Chasca Orkho series at Volcán Ollagüe, we must observe the petrologic textures of both the plagioclase feldspars and surrounding material in each sample. Host lava samples largely share similar petrologic textures and feldspar populations, with major and trace element core-to-rim transects depicting oscillating concentrations but remaining roughly the same (Figs. 6-8). However, our inclusion samples are split between textures and zonation similar to their host lava counterparts (Fig. 8) and a diktytaxitic texture with notable disequilibrium textures (Figs. 6-7). The petrologic observations and geochemical trends of the host lava and magmatic inclusions suggest we can better classify our intrusion samples as magmatic enclaves. We present this evidence as 1) the diktytaxitic texture of many of the inclusion samples; 2) the less silicic nature

of our inclusions in comparison to our host lava samples; and 3) the lack of a mineral assemblage or phenocryst size that would be found in a typical xenolith sample.

Plagioclase feldspar phenocrysts within host lava and enclave samples show distinct textural variations. Plagioclase phenocryst samples across host lava and enclave sample pairs show many similarities in zonation and textures, indicating that mixing between endmembers started to occur early in the evolution of the Chasca Orkho series. This phenomenon is within sample pair OLA-90-26/26i (Fig. 7). Both samples contain plagioclase populations predominantly containing patchy cores with oscillatory zoning out to the rims. Disequilibrium textures such as resorbance and sieving are seen in the cores of select phenocrysts. Therefore, the magmas represented by OLA-90-26/26i intermingled towards the beginning of their evolution represented by the disequilibrium textures in the cores, and then hybridized while recording slight variations in temperature and pressure the rest of their evolution, represented by the tight oscillatory zones in the mantles and rims.

The disequilibrium textures of the plagioclase observed in magmatic enclave samples OLA-90-15i and OLA-90-21iA indicate less time between the introduction of their representative magmas into the system and the eruption of the Chasca Orkho series. Plagioclase phenocrysts observed in these samples have large sections of disequilibrium textures within their mantles and rims, a clear distinction from plagioclase in samples OLA-90-26/26i (Figs. 6-8). Plagioclase phenocrysts from these magmatic enclave samples have little to no zoning with the exception of a core and a rim of varying size, suggesting that these samples have not experienced the same evolution as their counterparts. Therefore, the magmatic material that these plagioclase phenocrysts are derived from was thrown into disequilibrium when introduced to a host lava with a period of time for both sample types to begin hybridization, but not complete the process.

Mixing Between samples

Plagioclase feldspar major and trace element data in Figures 5, 10, and 11 present strong evidence of mixing between host lava and magmatic enclave samples, complementing the petrologic textures above. Trace element values normalized to chondrite suggest sample pair OLA-90-26 and OLA-90-26i share the same petrologic texture and feldspar zonation and represent the most homogeneous pair of samples (Fig. 5). In comparison, sample pairs OLA-90-15/15i and OLA-90-21/21iA have diktytaxitic enclave textures and pronounced disequilibrium within feldspars; feldspars from these samples have marked differences between each other and more variation than sample pair OLA-90-26/26i (Fig. 5). Notably, analyzed plagioclase feldspars from sample OLA-90-21 depict two separate signatures, inferring separate populations of the mineral phase which we interpret as evidence of mixing between the host lava and enclave pair (Fig. 5).

These strong mixing trends continue to be observed within trace element concentrations (Fig. 11). Most notably, a triangular trend is observed in plagioclase trace element concentrations, suggesting three compositional endmembers. The samples with the most points concentrated, on average, within these cruxes are samples OLA-90-15, OLA-90-21iA, and OLA-90-15i. While there are individual data from other samples (e.g., OLA-90-26) that have more extreme concentrations, data from the samples described above better represent the overall endmember compositions. The vast majority of plagioclase feldspar from samples are interpreted as originating from a mixture between a large volume (40%-80%) of magma best represented by OLA-90-15i with notably smaller volumes of magma from the other endmember compositions (Fig. 11; 15 = 0%-40%; OLA-90-21iA = 0%-50%). Plagioclase core analyses from host lava

samples almost exclusively range between the OLA-90-15 and OLA-90-15i endmembers (95%-20%) with minimal influence from the endmember represented by sample OLA-90-21iA (0%-20%; Fig. 11). Likewise, feldspar mantle analyses from the same host lava plagioclase samples show similar mixing trends as their cores with little to no change. Finally, the rims of these host lava plagioclase samples do show somewhat of a deviation from the mixing trends of the cores and mantles (Fig. 11). While rims of plagioclase from sample OLA-90-26 show little change in mixing trends, plagioclase rims from sample OLA-90-15 show an increasing interaction with the endmember represented by OLA-90-21iA from 5% or less to 15%-20% (Fig. 11). Additionally, plagioclase rims from sample OLA-90-21 show a marked increase of influence from the endmember represented by sample OLA-90-21iA (30%-45%; Fig. 11). This indicates that the endmembers represented by sample OLA-90-15 and OLA-90-15i were already established in the Chasca Orkho reservoir before the OLA-90-21iA endmember was introduced prior to eruption.

Trace element data from plagioclase cores originating from magmatic enclave samples have mixing trends that put them close to the endmember compositions represented by sample OLA-90-15i (95%-60%) with some influence of the OLA-90-15 endmember (0%-40%). The endmember represented by sample OLA-90-21iA does have some influence within this core population (0%-25%), but not a significant influence even within 21iA plagioclase cores (Fig. 11). This indicates that the magma endmember is best represented by sample OLA-90-21iA could have been slowly introduced into the shallow reservoir and absorbed plagioclase phenocrysts that did not originate from the magma body itself. Plagioclase mantles from magmatic enclave samples depict a significant increase in influence from the OLA-90-21iA endmember within the plagioclase phenocrysts that were found within the sample (Fig. 11). However, plagioclase mantles from samples OLA-90-15i and OLA-90-26i show little to no

change in their own mixing trends (Fig. 11). This could be explained by the different timescales of the plagioclase phenocrysts themselves; if phenocrysts from samples OLA-90-15i and OLA-90-21iA were formed and introduced to the Chasca Orkho reservoir earlier, it would explain why there is little to no sign of influence from the OLA-90-21iA endmember. The rims of the magmatic enclave plagioclase phenocrysts share similar trends with those of the mantles; little to no change in mixing trends is observed within plagioclase phenocryst rims of the magmatic enclaves.

Magma Reservoir Model

Within the Andean CVZ, much debate has been given to magmatic sourcing, evolution, and mixing at volcanic centers (Feeley et al., 1993; Feeley & Davidson, 1994 Michelfelder et al., 2013; Godoy et al., 2014, 2017; Blum-Oeste & Wörner, 2016; Taussi et al., 2019; Barnes et al., 2021; Rosenbaum et al., 2021). One aspect of this debate is how magma reservoirs are structured prior to eruption, either through a compositionally stratified magma chamber or a largely homogeneous reservoir with a single recharge event triggering an eruption. Compositionally stratified magma chambers are shallow reservoirs where eruptible material is stored within different 'layers' from least silicic (bottom) to most silicic (top) and have been utilized to describe magma systems in volcanic regions around the world (Riehle et al., 1992; Feeley et al., 2008; Taussi et al., 2019). With the mixing trends observed within the Chasca Orkho samples and the interpretation of multiple endmembers within the magma reservoir, we can infer that the reservoir that contained the Chasca Orkho series was compositionally stratified.

Within this shallow reservoir, we interpret magma represented by host lava sample OLA-90-15 to be the upper layer of the reservoir prior to eruption. This is supported by 1) low molar

An content in sampled plagioclase feldspar phenocrysts; 2) relative separation of trace element trends in comparison to other samples; and 3) the little overlap between plagioclase phenocrysts from OLA-90-15 and its enclave pair OLA-90-15i (Figs. 9-10, 12). When considering its position as a general endmember in Figure 11, we believe that the magma represented by sample OLA-90-15 originated from a hybridization and mixing reservoir and stands as a proxy of the rhyodacitic endmember represented in Central Andean magmatism (Blum-Oeste & Wörner, 2016).

Other host lava samples OLA-90-26 and OLA-90-21 do not have the separation from their corresponding magmatic enclave samples as OLA-90-15. Indeed, most of the plagioclase feldspar phenocrysts have the same range in values as those phenocrysts in their corresponding magmatic enclave samples. However, the small, shared range in trace element concentrations for sample pair OLA-90-26/26i (Figs. 5-8, 11) show extensive homogenization and mixing between the two magmas. Additionally, core-to-rim trace element transect analysis shows near identical Sr/Ba ratios of sampled plagioclase phenocrysts within both samples, indicating that these phenocrysts resided in equilibrium in a hybridized melt. This hybridization indicates that these two magmas spent a much longer time intermingling in comparison to sample pair OLA-90-15/15i. Considering this evidence, magma represented by OLA-90-15i is probably positioned below the magma represented by OLA-90-15, with the corresponding enclave sample OLA-90-26i representing a disaggregated layer of the stratified magma chamber. This recharge event represented by OLA-90-26i was most likely a prior recharge event that did not lead to eruption and instead hybridized with the magma already emplaced within the chamber, leading to the creation of magma represented by OLA-90-26 (Fig. 12). This recharge event would have

originated from a separate chamber, leading to the introduction of another compositional endmember within the Chasca Orkho series reservoir (Fig. 12).

In contrast to sample pair OLA-90-26/26i, magma represented by samples OLA-90-21/21iA appear to have a more complicated mixing history. This sample pair appears to have similar ranges in major and trace element concentrations (Figs. 9 and 11) yet also retain two separate plagioclase phenocryst populations inherited from endmembers (Figs. 5 and 11). This would indicate that some of these plagioclase phenocrysts were influenced by the introduction of a new magma that had limited time for significant hybridization. Additionally, the enclave sample OLA-90-21iA appears to show trace element concentrations similar to that of sample OLA-90-15i, representing a possible second recharge magma (Fig. 11). When observing sample OLA-90-21iA in thin section, the diktytaxitic fabric of the sample is punctuated with larger phenocrysts with extensive disequilibrium throughout the cores, mantles, and rims. We interpret sample OLA-90-21iA as containing plagioclase feldspar phenocrysts from its host lava counterpart but having its origins within a separate recharge event.

The last two samples of note, OLA-90-15i and OLA-90-21iA, contain plagioclase feldspar phenocrysts that have the highest molar An content (Fig. 9 and 12), have similar diktytaxitic petrologic textures and plagioclase zonation (Fig. 3-5), and trace element trends distinct from trends represented by OLA-90-15, and OLA-90-21/26/26i (Fig. 11). Therefore, we believe that these samples represent less silicic magma that was introduced into the shallow reservoir and triggered the eruption of the Chasca Orkho series. This magma was able to mix enough with plagioclase from sample OLA-90-21 to create two populations of rims and reached the top of the reservoir where magma represented by sample OLA-90-15 resided. However, eruption of the reservoir occurred before any substantial hybridization between OLA-90-15 and

OLA-90-15i could occur, explaining why there is so little overlap in composition between the sample pair.

With these observations, the evolution of the Chasca Orkho series prior to eruption can be split into three events concerning three endmembers: 1) The establishment of an evolved magma within the Chasca Orkho shallow reservoir; 2) the introduction of a basaltic andesitic endmember, creating the primary mixing trend seen through trace element concentrations (Fig. 11); and 3) introduction of a hybridized magma with influences from a primitive magma representing the third endmember. The establishment of the Chasca Orkho shallow reservoir begins with the emplacement of a magma body whose composition is best represented by sample OLA-90-15 and resembles the rhyodacitic endmember established by Blum-Oeste & Wörner, (2016). This magma continued to differentiate, becoming the most silicic endmember of the Chasca Orkho series. After a time, magma from basaltic andesitic source was introduced into the Chasca Orkho reservoir, creating the main mixing trend (Figs. 11-12). This new endmember is best represented by sample OLA-90-15 and resembles the basaltic andesitic endmember described in the CVZ (Blum-Oeste & Wörner, 2016). Due to this endmember's distinct geochemical signature, it would have originated from an isolated source separate from the hybridization chamber (Fig. 12). The introduction of this source would have created the stratified structure of the Chasca Orkho shallow reservoir while the temperature differences between the most evolved endmember would account for the diktytaxitic petrology of magmatic enclave sample OLA-90-15i. Much of the magma within the shallow reservoir was heavily influenced by this endmember and the compositions for much of the plagioclase feldspar phenocrysts in samples OLA-90-15i, OLA-90-21, OLA-90-26, and OLA-90-26i resulted (Fig. 12). The third endmember from this system introduced into the Chasca Orkho shallow reservoir is best

represented by sample OLA-90-21iA would be introduced to the system. This endmember likely originated from the hybridizing and mixing chamber that our first endmember originated from due to the intermediate range of molar An contents of plagioclase from the sample as well as the similar range in Sr/Ba ratios (Figs. 11-12). However, by this time the hybridization chamber sourcing the Chasca Orkho reservoir had new magmatic influences resembling the enriched basalt endmember in Blum-Oeste & Wörner, (2016). This endmember aided in changing the overall magmatic signature of the hybridization reservoir, but the endmember's geochemistry itself was diluted. This would explain the relatively small influence this endmember has on the Chasca Orkho shallow reservoir (Fig. 11). The introduction of magma from the altered hybridization reservoir most likely triggered the disequilibrium of the Chasca Orkho shallow reservoir as 1) only one other sample (OLA-90-21) was significantly influenced by it; 2) the small size and observations of disequilibrium textures within its plagioclase; and 3) the populations of plagioclase phenocrysts within the sample did not have enough time to hybridize along the second major mixing trend.

CONCLUSIONS

Magmatic mixing and evolution in the Andean Central Volcanic Zone is often complex, with magma originating from multiple sources before forming an intermediate hybrid prior to eruption. At Volcán Ollagüe, we utilized whole rock chemistry, plagioclase feldspar phenocryst chemistry, and petrologic textures to gain understanding of the magmatic evolution of the Chasca Orkho series host lava and magmatic inclusions.

Observations of thin sections of magmatic inclusion samples indicate that these inclusions can be classified as magmatic enclaves due to the diktytaxitic petrologic texture and the geochemical signatures of the whole rock and plagioclase feldspar phenocrysts analyzed in this study. These magmatic enclaves therefore represent magma mixing between magmatic components, or endmembers, to create the geochemical nature of the Chasca Orkho lava series. Additionally, the petrology of magmatic enclave sample OLA-90-26i and its similarity to host lava petrology infers disaggregation of a stratified magma chamber.

From the results of this study, a compositionally stratified magma chamber with three distinct geochemical endmember influences is interpreted. The first endmember emplaced within the Chasca Orkho shallow reservoir originates from a hybridization chamber and begins to fractionate, creating the most evolved endmember of the Chasca Orkho series. Our second endmember is basaltic andesitic and best represented by sample OLA-90-15i, originating from an isolated chamber separate from the hybridization chamber. The interaction of these two endmembers creates the stratified structure of the Chasca Orkho shallow reservoir as well as the enclaves that eventually form samples OLA-90-15, OLA-90-15i, OLA-90-26, and OLA-90-26i.

At the same time, the hybridization chamber from which our first endmember originates begins to be influenced by a third and final geochemical endmember which is eventually introduced into the Chasca Orkho shallow reservoir.

REFERENCES

Barnes, C.G., Werts, K., Memeti, V., Paterson, S.R., Bremer, R., 2021, A tale of five enclaves: Mineral perspectives on origins of mafic enclaves in the Tuolumne Intrusive Complex: Geosphere, v.17, no.2, p.352-374, doi:10.1130/GES02233.1

Blum-Oeste, M., Wörner, G., 2016, Central Andean magmatism can be constrained by three ubiquitous end-members: Terra Nova, v.28, p.434-440, doi: 10.1111/trt.12237

Chadwick, J.P., Troll, V.R., Waight, T.E., van der Zwan, F.M., Schwarzkopf, L.M., 2013, Petrology and geochemistry of igneous inclusions in recent Merapi deposits: a window into the sub-volcanic plumbing system: Contributions to Mineralogy and Petrology, v.165, p.259-282, doi: 10.1007/s00410-012-0808-7

Chen, Z., Zeng, Z., Wang, X., Peng, X., Zhang, Y., Yin, X., Chen, S., Zhang, L., Qi, H., 2020, Element and Sr isotope zoning in plagioclase in the dacites from the southwestern Okinawa Trough: Insights into magma mixing processes and time scales: Lithos, v.376, p.105776, doi: https://doi.org/10.1016/j.lithos.2020.105776

Chew, D., Drost, K., Marsh, J.H., Petrus, J.A., 2021, LA-ICP-MS imaging in the geosciences and its applications to geochronology: Chemical Geology, v.559, p.1-23, doi: 10.1016/j.chemgeo.2020.119917

Chmielowski, J., Zandt, G., Haberland, C.,1999, The Central Andean Altiplano-Puna Magma Body: Geophysical Research Letters, v.26, no.6, p.783-786, doi: https://doi.org/ 10.1029/1999GL900078

Cooper, K.M., Kent, A.J.R., 2014, Rapid remobilization of magmatic crystals kept in cold storage: Nature, v.506, p.480-483, doi:10.1038/nature12991

Coote, A., Shane, P., Stirling, C., Reid, M., 2018, The origin of plagioclase phenocrysts in basalts from continental monogenetic volcanoes of the Kaikohe-Bay of Islands field, New Zealand: implications for magmatic assembly and ascent: Contributions to Mineralogy and Petrology, v.173, no.14, p.1-19, doi:10.1007/s00410-018-1440-y

Davidson, J.P., Morgan, D.J., Charlier, B.L.A., 2007b, Isotopic Microsampling of Magmatic Rocks: Elements, v.3, p.253-259, doi: https://doi.org/10.2113/gselements.3.4.253

Davidson, J.P., Morgan, D.J., Charlier, B.L.A., Harlou, R., Hora, J.M., 2007a, Microsampling of Isotopic Analysis of Igneous Rocks: Implications for the Study of Magmatic Systems: Annual Review of Earth and Planetary Sciences, v.35, p.273-311, doi: 10.1146/ annurev.earth.35.031306.140211

De Silva, S.L., 1989, Altiplano-Puna volcanic complex of the central Andes: Geology, v.17, no.12, p.1102-1106, doi: 10.1130/0091-7613(1989)017<1102:APVCOT>2.3.CO;2

Feeley, T.C., Davidson, J.P., 1994, Petrology of Calc-Alkaline Lavas at Volcán Ollagüe and the Origin of Compositional Diversity at Central Andean Stratovolcanoes: Journal of Petrology, v.35, no.5, p.1295-1340, doi: https://doi.org/10.1093/petrology/35.51295

Feeley, T.C., Davidson, J.P., Armendia, A., 1993, The volcanic and magmatic evolution of Volcán Ollagüe, a high-K, late Quaternary stratovolcano in the Andean Central Volcanic Zone: Journal of Volcanology and Geothermal Research, v.54, p.221-245, doi: https://doi.org/10.1016/0377-0273(93)90065-Y

Feeley, T.C., Hacker, M.D., 1995, Intracrustal Derivation of Na-Rich Andesitic and Dacitic Magmas: An Example from Volcán Ollagüe, Andean Central Volcanic Zone: Journal of Geology, v.103, no.2, p.213-225, doi: https://doi/org/10.1086/629737

Feeley, T.C., Sharp, Z.D., 1995, $^{18}O/^{16}O$ isotope geochemistry of silicic lava flows erupted from Volcán Ollagüe, Andean Central Volcanic Zone: Earth and Planetary Science Letters, v.133, p. 239-254, doi: https://doi.org/10.1016/0012-821X(95)00094-S

Feeley, T.C., Wilson, L.F., Underwood, S.J., 2008, Distribution and compositions of magmatic inclusions in the Mount Helen dome, Lassen Volcanic Center, California: Insights into magma chamber processes: Lithos, v.106, p. 173-189, doi: 10.1016/j.lithos.2008.07.010

Font, L., Davidson, J.P., Pearson, D.G., Nowell, G.M., Jerram, D.A., Ottley, C.J., 2008, Sr and Pb Isotope Micro-analysis of Plagioclase Crystals from Skye Lavas: and Insight into Open-system Processes in a Flood Basalt Province: Journal of Petrology, v.49, no.8, p.1449-1471, doi:10.1093/petrology/egn032

Ginibre, C., Davidson, J.P., 2014, Sr Isotope Zoning in Plagioclase from Parinacota Volcano (Northern Chile): Quantifying Magma Mixing and Crustal Contamination: Journal of Petrology, v.55, p.1203-1238, doi:10.1093/petrology/egu023

Ginibre, C., Wörner, G., 2007, Variable parent magmas and recharge regimes of the Parinacota magma system (N. Chile) revealed by Fe, Mg and Sr zoning in plagioclase: Lithos, v.98, p.118-140, doi: 10.1016/j.lithos.2007.03.004

Gregory-Wodzicki, K.M., 2000, Uplift history of the Central and Northern Andes: A review: GSA Bulletin, v.112, p.1091-1105, doi: https://doi.org/10.1130/0016760 6(2000)112%3C1091:UHOTCA%3E2.0.CO;2

Hildreth, W., Moorbath, S., 1988, Crustal contributions to arc magmatism in the Andes of Central Chile: Contributions to Mineralogy and Petrology, v.98, p.455-489, doi: https://doi.org/10.1007/BF00372365

Jackson, M.D., Blundy, J., Sparks, R.S.J., 2018, Chemical differentiation, cold storage and remobilization of magma in the Earth's crust: Nature, v.564, p.405-409, doi: https://doi.org/10.1038/s41586-018-0746-2

Jochum, K.P., Weis, U., Stoll, B., Kuzmin, D., Yang, Q., Raczek, I., Jacob, D.E., Stracke, A., Birbaum, K., Frick, D.A., Günther, D., Enzweiler, J., 2011, Determination of Reference Values for NIST-SRM 610-617 Glass Following ISO Guidelines: Journal of Geostandards and Geoanalytical Research, v.31, p. 397-429, doi: 10.1111/j.1751-908X.2011.00120.x

Kent, A.J.R., 2013, Preferential eruption of andesitic magmas: Implications for volcanic magma fluxes at convergent margins: London Geological Society, Special Publications, v.385, p.257-280, doi: https://doi.org/10.1144/SP385.10

Kent, A.J.R., Darr, C., Koleszar, A.M., Salisbury, M.J., Cooper, K.M., 2010, Preferential eruption of andesitic magmas through recharge filtering: Nature Geoscience, v.3, p.631-636, doi: 10.1038/NGEO924

Klemetti, E.W., Clynne, M.A., 2014, Localized Rejuvenation of a Crystal Mush Recorded in Zircon Temporal and Compositional Variation at the Lassen Volcanic Center, Northern California: PLoS ONE, v.9, no.12, doi:10.1371/journal.pone.0113157

Laviada-Garmon, D., 2022, Chemical and Thermal Influence on Intermediate Magma Storage Conditions: Volcán Ollagüe, Chile-Bolivia, Central Andes [M.Sc. Thesis]: Springfield, Missouri State University, 81p.

Lormand, C., Zellmer, G.F., Sakamoto, N., Ubide, T., Kilgour, G., Yurimoto, H., Palmer, A., Németh, K., Iizuka, Y., Moebis, A., 2021, Shallow magmatic processes revealed by cryptic micoantecrysts: a case study from the Taupo Volcanic Zone: Contributions to Mineralogy and Petrology, v.176, no.97, doi: 10.1007.s00410-021-01857-7

Michelfelder, G.S., Feeley, T.C., Wilder, A.D., Klemetti, E.W., 2013, Modification of the Continental Crust by Subduction Zone Magmatism and Vice-Versa: Across-Strike Geochemical Variations of Silicic Lavas from Individual Eruptive Centers in the Andean Central Volcanic Zone: Geosciences, v.3, p.633-667, doi: 10.3390/geosciences3040633

Paton, C., Hellstrom, J., Paul, B., Woodhead, J., Hergt, J., 2011, Iolite: Freeware for the visualisation and processing of mass spectrometric data: Journal of Analytical Atomic Spectrometry, v.26, p.2508-2518, doi: 10.1039/C1JA10172B

Perkins, J.P., Ward, K.M., de Silva, S.L., Zandt, G., Beck, S.L., Finnegan, N.J., 2016, Surface uplift in the Central Andes driven by growth of the Altiplano Puna Magmatic Body: Nature Communications, v.7, p.1-10, doi: 10.1038/ncomms13185

Pritchard, M.E., de Silva, S.L., Michelfelder, G., Zandt, G., McNutt, S.R., Gottsman, J., West, M.E., Blundy, J., Christensen, D.H., Finnegan, N.J., Minaya, E., Sparks, R.S.J., Sunagua,

M., Unsworth, M.J., Alvizuri, C., Comeau, M.J., del Potro, R., Díaz, D., Diez, M., Farrell, A., Henderson, S.T., Jay, J.A., Lopez, T., Legrand, D., Naranjo, J.A., McFarlin, H., Muir, D., Perkins, J.P., Spica, Z., Wilder, A., Ward, K.M., 2018, Synthesis: PLUTONS: Investigating the relationship between pluton growth and volcanism in the Central Andes: Geosphere, v.14, no.3, 954-957, doi: 10.1130/GES01578.1

Riehle, J.R., Champion, D.E., Brew, D.A., Lanphere, M.A., 1992, Pyroclastic deposits of the Mount Edgecumbe volcanic field, southeast Alaska: eruptions of a stratified magma chamber, Journal of Volcanology and Geothermal Research, v.53, p.117-143, doi: 10.1016/0377-0273(92)90078-R

Rosenbaum, G., Caulfield, J.T., Ubide, T., Ward, J.F., Sandiford, D., Sandiford, M., 2021, Spatially and Geochemically Anomalous Arc Magmatism: Insights from the Andean Arc: Geochemistry, Geophysics, Geosystems, v.22, p.1-22, doi: 10.1029/2021GC009688

Salisbury, M.J., Jicha, B.R., de Silva, S.L., Singer, B.S., Jiménez, N.S., Ort, M.H., 2011, 40Ar/39Ar chronostratigraphy of Altiplano—Puna volcanic complex ignimbrites reveals the development of a major magmatic province: GSA Bulletin, v.123, no.5, p.821-840, doi: 10.1130/B30280.1

Shane, P., Cocker, K., Coote, A., Stirling, C.H., Reid, M.R., 2019, The prevalence of plagioclase antecrysts and xenocrysts in andesite magma, exemplified by lavas of the Tongariro volcanic complex, New Zealand: Contributions to Mineralogy and Petrology, v.174, no.89, p.1-18, doi:10.1007/s00410-019-1626-y

McDonough, W.F., Sun, S.S., 1995, The composition of the Earth: Chemical Geology, v.120, no.3-4, p.223-253, doi: 10.1016/0009-2541(94)00140-4

Taussi, M., Godoy, B., Piscaglia, F., Morata, D., Agostini, S., Le Roux, P., González-Maurel, O., Gallmeyer, G., Menzies, M., Renzulli, A., 2019, The upper crustal magma plumbing system of the Pleistocene Apacheta-Aguilucho Volcanic Complex area (Altiplano-Puna, northern Chile) as inferred from the erupted lavas and their enclaves: Journal of Volcanology and Geothermal Research, v.373, p.179-198, doi: 10.1016/j.jvolgeores.2019.01.021

Tepley III, F.J., Davidson, J.P., Clynne, M.A., 1999, Magmatic Interactions as Recorded in Plagioclase Phenocrysts of Chaos Crags, Lassen Volcanic Center, California: Journal of Petrology, v. 40, no. 5, p.787-806, doi: https://doi.org/10.1093/petroj/40.5.787

Tepley III, F.J., Davidson, J.P., Tilling, R.I., Arth, J.G., 2000, Magma Mixing, Recharge, and Eruption Histories Recorded in Plagioclase Phenocrysts from El Chichón Volcano, Mexico: Journal of Petrology, v.41, no.9, p.1397-1411, doi: https://doi.org/10.1093 /petrology/41.9.1397

Tibaldi, A., Bistacchi, A., Pasquaré, F.A., Vezzoli, L., 2006, Extensional tectonics and volcano lateral collapses: insights from Ollagüe volcano (Chile-Bolivia) and analogue modelling: Terra Nova, v.18, p.282-289, doi: 10.1111/j.1365-3121.2006.00691.x

Ubide, T., Larrea, P., Becerril, L., Galé, C., 2021a, Volcanic plumbing filters on ocean-island basalt geochemistry, Geology, v.50, no.1, p.26-31, doi: 10.1130/G49224.1

Ubide, T., Neave, D.A., Petrelli, M., Longré, M., 2021b, Editorial: Crystal Archives of Magmatic Processes: Frontiers in Earth Science, v.9, p.1-7, doi:10.3389/feart.2021.749100

Vezzoli, L., Tibaldi, A., Renzulli, A., Menna, M., Flude, M., 2008, Faulting-assisted lateral collapses and influence on shallow magma feeding system at Ollagüe volcano (Central Volcanic Zone, Chile-Bolivia Andes: Journal of Volcanology and Geothermal Research, v.171, p.137-159, doi: 10.1016/j.jvolgeores.2007.11.015

Ward, Kevin M., Zandt, George, Beck, Susan L., Christensen, Douglas H., McFarlin, Heather, 2014, Seismic imaging of the magmatic underpinnings beneath the Altiplano-Puna volcanic complex from the joint inversion of surface wave dispersion and receiver functions: Earth and Planetary Science Letters, v.404, p.43-53, doi: https://dx.doi.org/10.1016/j.epsl.2014.07.022

Woodhead, J., Hellstrom, J., Hergt, J., Greig, A., Maas, R., 2007, Isotopic and elemental imaging of geological materials by laser ablation Inductively Couple Plasma mass spectrometry: Journal of Geostandards and Geoanalytical Research, v.31, p.331-343, doi: 10.1111/j.1751-908X.2007.00104.x

Zhang, J., Davidson, J.P., Humphreys, M.C.S., Macpherson, C.G., Neill, I., 2015, Magmatic Enclaves and Andesitic Lavas from Mt. Lamington, Papua New Guinea: Implications for Recycling of Earlier-fractionated Minerals through Magma-Recharge: Journal of Petrology, v.56, no.11, p.2223-2256, doi: 10.1093/petrology/evg071

Table 1. Summary of trace element chemistry for all whole rock samples

Whole Rock Trace Element Chemistry from ICP-MS										
Sample ID	Sc (ppm)	Zn (ppm)	Rb (ppm)	Sr (ppm)	Y (ppm)	Zr (ppm)	Nb (ppm)	Cs (ppm)	Ba (ppm)	La (ppm)
OLA-90-3i	0	48.063	18.004	280.97	7.664	85.443	4.958	0.572	382.5	13.435
OLA-90-06	0	40.01	35.445	209.071	7.609	54.952	7.391	1.229	397.49	16.581
OLA-90-07	0	36.479	36.412	206.338	7.32	60.766	6.538	1.187	374.05	16.094
OLA-90-8i	0	53.12	37.541	304.264	8.947	95.222	7.385	0.887	430.38	17.132
OLA-90-13	0	44.772	39.571	192.651	8.281	70.067	17.225	1.38	403.91	17.199
OLA-90-13i	2.427	53.226	33.122	349.039	6.185	29.253	5.648	1.844	521.21	10.348
OLA-90-15	0	34.996	46.227	176.763	5.014	37.827	7.289	1.977	473.47	19.688
OLA-90-15i	0	62.371	26.322	329.635	10.889	74.157	6.496	0.646	470.1	16.598
OLA-90-20	0	37.094	50.208	189.07	5.955	45.889	7.038	2.631	399.7	16.798
OLA-90-21	2.414	127.543	65.086	403.742	14.45	166.81	11.014	2.268	599.13	34.363
OLA-90-21iA	0	41.919	18.4	291.093	8.307	89.353	16.343	0.904	391.56	13.029
OLA-90-25	0	37.679	44.856	189.165	5.948	54.335	7.349	2.339	388.61	16.395
OLA-90-25i	0	50.399	26.908	316.006	9.916	94.511	8.485	1.047	404.34	14.995
OLA-90-26	0	57.327	44.234	283.517	10.483	84.674	8.27	1.657	518.33	19.906
OLA-90-26i	0	44.212	18.764	189.698	8.875	68.986	5.105	0.509	281.49	12.466
OLA-90-27	0	40.935	39.639	186.112	6.739	42.457	4.728	1.284	392.94	17.178
OLA-90-27i	0	44.681	13.092	394.718	10.557	46.899	5.574	0.679	831.17	17.023
OLA-90-34	0	50.661	37.762	245.521	8.494	93.791	7.589	1.158	492.94	17.205
OLA-90-37	0	38.356	36.602	226.292	6.895	57.721	6.999	1.54	426.9	15.298
OLA-90-37i	0	52.312	30.975	365.734	10.36	96.48	5.813	0.733	377.12	16.058
OLA-90-41	0	70.196	59.2	352.447	12.289	93.771	10.339	1.873	606.05	23.657
OLA-90-45	0	33.825	19.632	168.68	5.435	59.377	2.871	0.698	253.99	11.689
OLA-90-46	0	43.552	52.98	208.861	7.974	63.394	7.185	1.745	419.51	19.196
OLA-90-48	0	38.819	32.263	240.903	7.604	71.953	8.577	1.259	414.49	16.358
OLA-90-48i	0	54.217	31.068	345.612	10.603	95.46	6.856	0.983	495.34	17.016
OLA-90-51	0	49.961	39.933	244.59	10.715	92.1	7.836	1.441	470.15	17.612
OLA-90-52	0	40.56	24.646	187.793	7.478	80.899	3.656	0.737	259.73	14.535

Table 1. Summary of trace element chemistry for all whole rock samples

Whole Rock Trace Element Chemistry from ICP-MS Continued										
Sample ID	Ce (ppm)	Pr (ppm)	Nd (ppm)	Sm (ppm)	Eu (ppm)	Gd (ppm)	Tb (ppm)	Dy (ppm)	Ho (ppm)	Er (ppm)
OLA-90-3i	30.059	10.393	13.281	2.638	0.695	1.822	0.286	1.489	0.261	0.707
OLA-90-06	40.56	11.697	14.66	2.776	0.696	1.933	0.298	1.456	0.242	0.834
OLA-90-07	36.815	11.583	14.243	2.674	0.661	1.843	0.282	1.364	0.235	0.752
OLA-90-8i	32.904	13.082	16.56	3.26	0.823	2.245	0.351	1.693	0.283	0.6
OLA-90-13	30.095	11.907	14.682	2.746	0.674	1.87	0.299	1.491	0.257	0.56
OLA-90-13i	37.43	5.987	7.328	1.31	0.741	1.124	0.169	0.935	0.188	1.115
OLA-90-15	35.432	11.452	13.749	2.506	0.58	1.639	0.235	1.088	0.177	0.537
OLA-90-15i	31.501	13.441	17.524	3.581	0.971	2.586	0.43	2.176	0.361	0.74
OLA-90-20	35.432	11.452	13.749	2.506	0.58	1.639	0.235	1.088	0.177	0.537
OLA-90-21	68.835	24.906	31.26	5.755	1.367	3.823	0.573	2.72	0.443	1.049
OLA-90-21iA	30.514	9.892	12.828	2.54	0.66	1.779	0.286	1.473	0.254	0.812
OLA-90-25	37.315	11.336	13.831	2.484	0.581	1.647	0.235	1.096	0.179	0.611
OLA-90-25i	42.147	11.393	14.596	2.899	0.818	2.129	0.346	1.841	0.328	1.147
OLA-90-26	48.831	14.5	18.028	3.467	0.879	2.465	0.383	1.932	0.329	1.131
OLA-90-26i	31.786	9.73	12.8	2.662	0.68	1.965	0.316	1.641	0.286	0.864
OLA-90-27	32.285	12.333	15.016	2.779	0.683	1.876	0.292	1.439	0.242	0.58
OLA-90-27i	42.149	12.128	14.777	2.709	0.86	2.074	0.343	1.909	0.367	1.36
OLA-90-34	30.451	12.404	15.435	2.963	0.83	1.989	0.324	1.635	0.277	0.618
OLA-90-37	37.052	10.888	13.131	2.488	0.671	1.778	0.271	1.359	0.228	0.781
OLA-90-37i	41.468	12.595	16.104	3.149	0.847	2.247	0.355	1.871	0.326	1.028
OLA-90-41	58.788	16.911	20.808	3.906	1.023	2.74	0.424	2.131	0.367	1.263
OLA-90-45	22.433	8.18	10.057	1.878	0.51	1.312	0.214	1.13	0.204	0.494
OLA-90-46	39.756	12.958	15.3	2.762	0.675	1.925	0.295	1.436	0.247	0.737
OLA-90-48	43.307	11.383	14.158	2.652	0.681	1.886	0.289	1.473	0.25	0.994
OLA-90-48i	42.983	12.533	15.793	3.096	0.833	2.216	0.349	1.805	0.316	1.049
OLA-90-51	47.983	12.567	15.751	3.063	0.767	2.239	0.357	1.848	0.328	1.204
OLA-90-52	27.033	10.989	13.509	2.562	0.612	1.775	0.291	1.526	0.272	0.67

Table 1. Summary of trace element chemistry for all whole rock samples

Whole Rock Trace Element Chemistry from ICP-MS Continued								
Sample ID	Tm (ppm)	Yb (ppm)	Lu (ppm)	Hf (ppm)	Ta (ppm)	Pb (ppm)	Th (ppm)	U (ppm)
OLA-90-3i	0.076	0.618	0.078	2.613	0.551	4.855	2.151	0.829
OLA-90-06	0.070	0.558	0.070	2.029	1.282	5.125	3.356	1.024
OLA-90-07	0.067	0.554	0.070	2.115	1.035	4.439	3.224	0.934
OLA-90-8i	0.076	0.590	0.074	3.079	1.214	4.522	2.790	0.766
OLA-90-13	0.073	0.590	0.074	2.805	1.685	5.326	3.998	1.190
OLA-90-13i	0.069	0.631	0.092	1.114	1.060	6.247	2.557	0.438
OLA-90-15	0.040	0.311	0.039	1.478	1.105	5.914	3.867	1.753
OLA-90-15i	0.091	0.680	0.078	2.572	0.557	4.082	1.847	0.402
OLA-90-20	0.053	0.445	0.056	1.796	1.226	6.330	4.294	2.486
OLA-90-21	0.125	1.018	0.129	4.893	0.983	12.634	6.418	3.641
OLA-90-21iA	0.077	0.626	0.082	3.351	1.438	4.759	3.170	1.103
OLA-90-25	0.053	0.441	0.057	2.014	1.455	6.200	4.258	2.345
OLA-90-25i	0.098	0.804	0.103	3.174	0.965	5.154	3.121	0.625
OLA-90-26	0.097	0.769	0.099	2.858	1.222	7.064	4.028	1.209
OLA-90-26i	0.081	0.668	0.082	2.345	0.592	3.416	1.880	0.422
OLA-90-27	0.069	0.556	0.068	1.618	0.420	5.635	2.903	1.159
OLA-90-27i	0.117	0.977	0.130	1.585	0.808	5.192	2.123	0.508
OLA-90-34	0.082	0.682	0.088	3.093	0.981	7.384	3.926	1.239
OLA-90-37	0.066	0.532	0.066	2.087	1.016	5.115	3.635	1.380
OLA-90-37i	0.095	0.761	0.098	3.000	0.646	4.394	2.858	0.769
OLA-90-41	0.106	0.871	0.108	3.211	1.385	8.319	5.129	1.434
OLA-90-45	0.063	0.508	0.068	1.940	0.170	3.665	1.973	0.681
OLA-90-46	0.074	0.600	0.076	2.211	0.924	6.660	4.614	1.325
OLA-90-48	0.074	0.580	0.075	2.573	1.207	5.495	3.293	0.871
OLA-90-48i	0.093	0.751	0.096	2.962	0.823	5.515	2.703	0.729
OLA-90-51	0.100	0.822	0.105	2.934	1.190	5.444	3.549	1.217
OLA-90-52	0.084	0.690	0.088	2.468	0.214	5.010	2.497	1.008

Table 2.Major Element Concentration Range for Plagioclase Feldspar per Sample

Sample ID	SiO_2 wt%	Al_2O_3 wt %	Na_2O wt%	MgO wt%	FeO wt%	TiO_2 wt%	K_2O wt%	CaO wt%	Molar An %
OLA-90-15 Min	58.36	23.51	6.30	0	0.156	0	0.56	5.35	26.23
OLA-90-15 Max	62.17	25.77	8.07	0.021	0.315	0.048	0.95	7.99	39.76
OLA-90-15i Min	52.10	25.00	4.04	0.004	0.179	0	0.16	7.63	38.86
OLA-90-15i Max	60.11	29.85	6.72	0.044	0.515	0.058	0.55	12.58	62.52
OLA-90-20 Min	55.65	22.62	5.50	0.006	0.239	0	0.38	5.68	29.93
OLA-90-20 Max	63.12	28.44	7.24	0.034	0.479	0.081	0.94	10.29	49.72
OLA-90-20i Min	52.23	24.29	4.03	0.001	0.199	0	0.23	5.64	26.99
OLA-90-20i Max	61.43	30.55	7.72	0.025	0.384	0.069	1.08	13.15	63.45
OLA-90-21 Min	55.34	24.07	4.98	0	0.149	0	0.51	6.40	32.42
OLA-90-21 Max	60.48	27.65	6.55	0.043	0.424	0.042	1.26	10.49	52.17
OLA-90-21iA Min	51.32	24.55	3.43	0	0.165	0	0.19	6.99	34.69
OLA-90-21iA Max	60.06	29.75	6.94	0.081	0.819	0.056	0.77	13.90	68.33
OLA-90-26 Min	52.09	25.13	4.17	0	0.206	0	0.26	6.80	33.08
OLA-90-26 Max	60.33	30.23	7.05	0.029	0.410	0.075	0.96	12.62	61.49
OLA-90-26i Min	53.53	25.29	4.68	0	0.202	0	0.35	7.12	34.39
OLA-90-26i Max	59.80	29.24	6.94	0.049	0.510	0.072	0.86	11.60	56.56

Table 3. Trace Element Concentration Range for Plagioclase Feldspar per Sample

Sample ID	Li (ppm)	Mg (ppm)	Fe (ppm)	Sr (ppm)	Ba (ppm)	Ce (ppm)	Nd (ppm)	Sm (ppm)	Eu (ppm)	Pb (ppm)
OLA-90-15 Min	18.403	58.429	1053.824	1164.545	339.547	12.045	1.475	0.154	0.914	10.292
OLA-90-15 Max	93.109	26747.814	2082.098	2985.430	1269.185	55.858	17.479	2.706	4.022	31.499
OLA-90-15i Min	2.625	99.228	870.394	1351.879	158.664	6.027	1.847	0.158	0.528	1.559
OLA-90-15i Max	17.423	248.889	1526.134	2015.388	476.496	52.729	29.344	5.015	1.726	5.978
OLA-90-21 Min	19.043	99.430	1056.100	1082.513	265.023	10.731	2.054	0.142	1.063	4.753
OLA-90-21 Max	39.963	715.540	3072.632	1748.314	1562.672	81.577	39.379	6.932	3.338	28.541
OLA-90-21iA Min	8.333	59.250	798.210	1035.966	195.603	8.262	2.040	0.120	0.685	3.440
OLA-90-21iA Max	41.810	5270.027	7167.624	1597.874	972.015	93.209	49.495	8.869	2.419	23.235
OLA-90-26 Min	8.629	97.098	1028.706	857.684	129.758	5.151	1.617	0.236	0.835	7.454
OLA-90-26 Max	20.734	5980.383	6077.239	1554.978	720.693	36.480	11.318	2.023	2.330	19.262
OLA-90-26i Min	14.347	86.166	1090.879	1143.943	229.102	14.982	3.556	0.282	0.965	8.004
OLA-90-26i Max	23.180	255.393	3334.691	1591.559	854.983	129.401	8.997	1.031	2.317	30.491

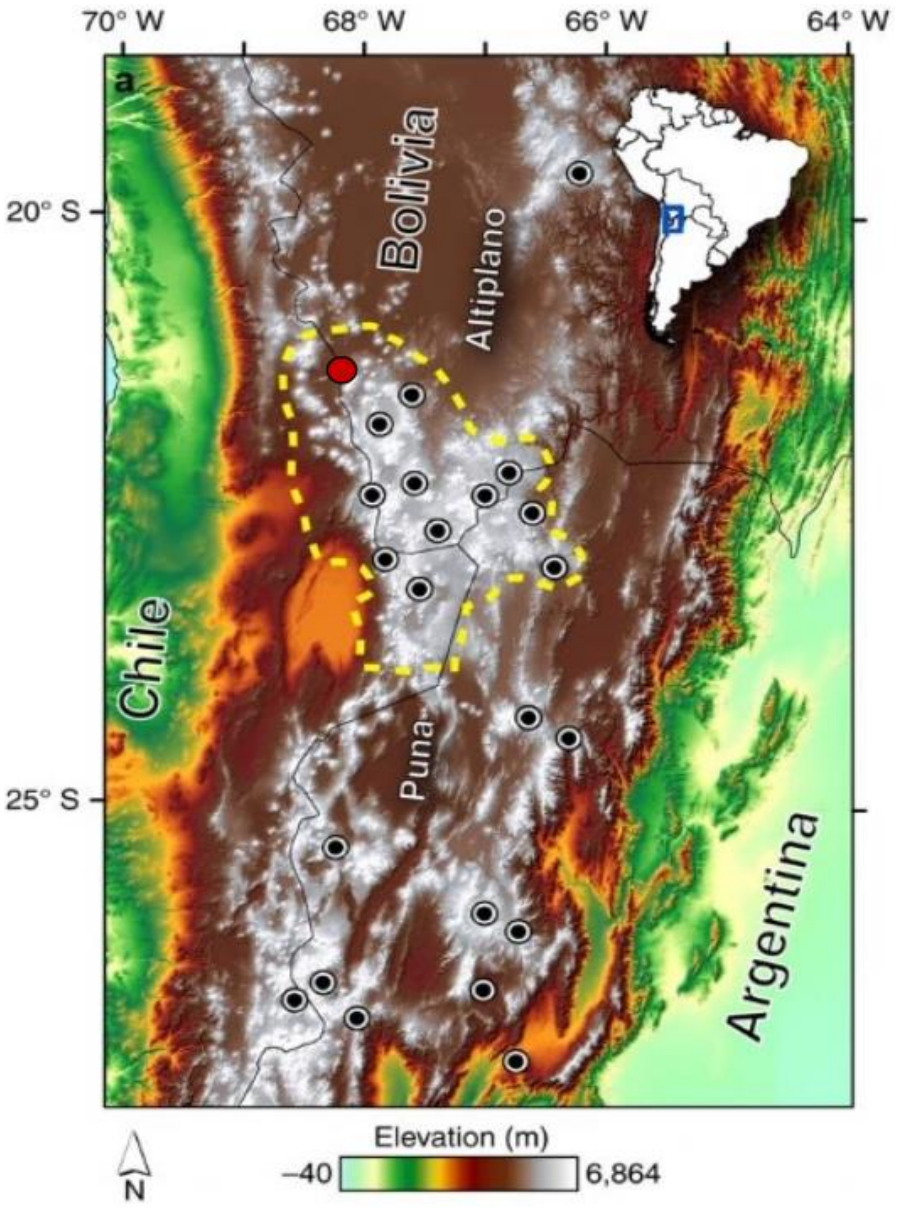

Figure 1: The location of Volcán Ollagüe within the Central Andes and the Altiplano-Puna Volcanic Complex (yellow). Volcán Ollagüe is represented by the red dot in the northwest of the APVC. Adapted from Perkins et al. (2016)

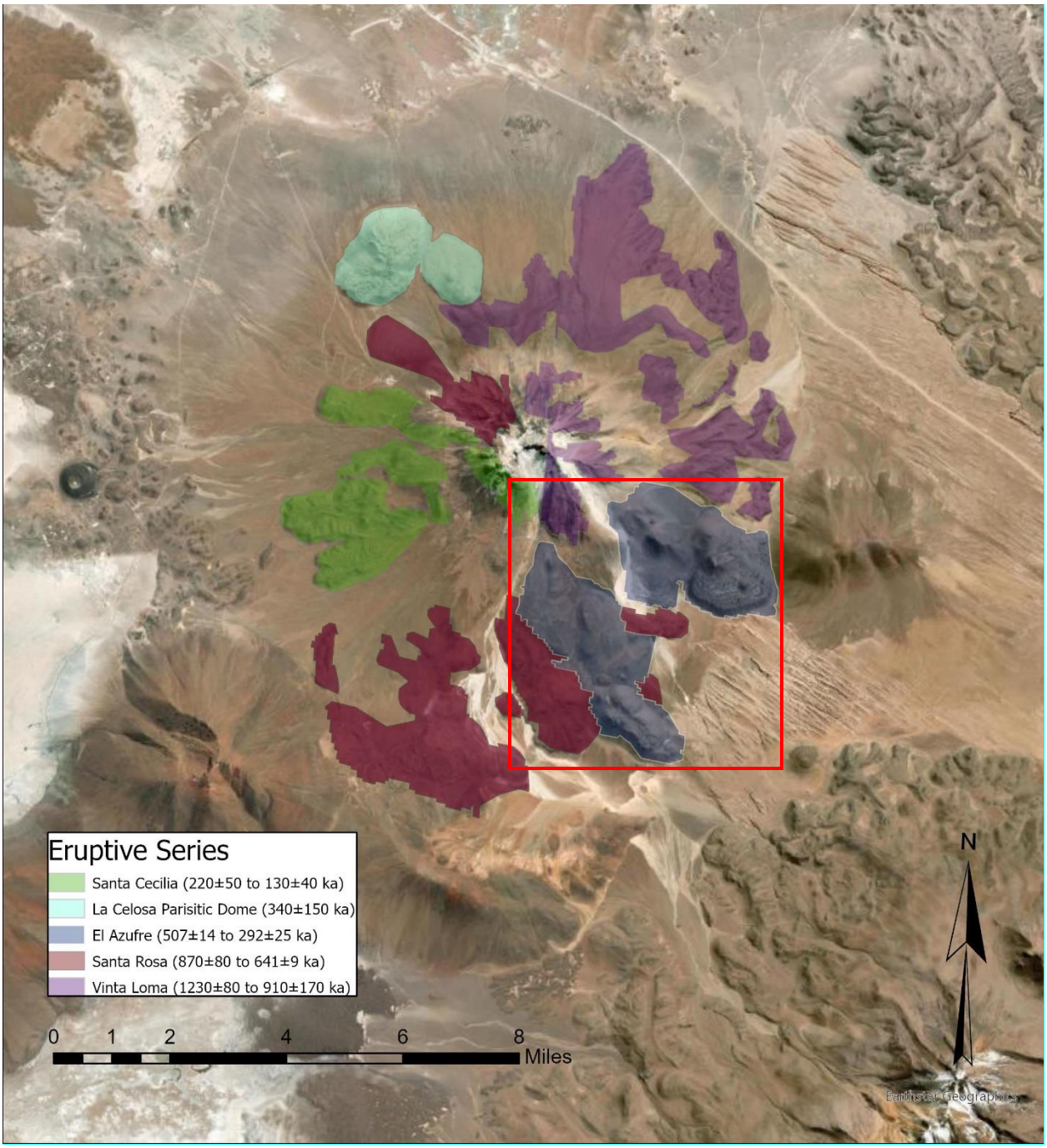

Figure 2: Representation of Volcán Ollagüe's four major eruptive series as classified by Vezzoli et al. (2008). This study focuses on the Chasca Orkho flank eruptions (red box) within the El Azufre lava series due to its large and prolific magmatic enclaves. Figure adapted from Laviada-Garmon (2022).

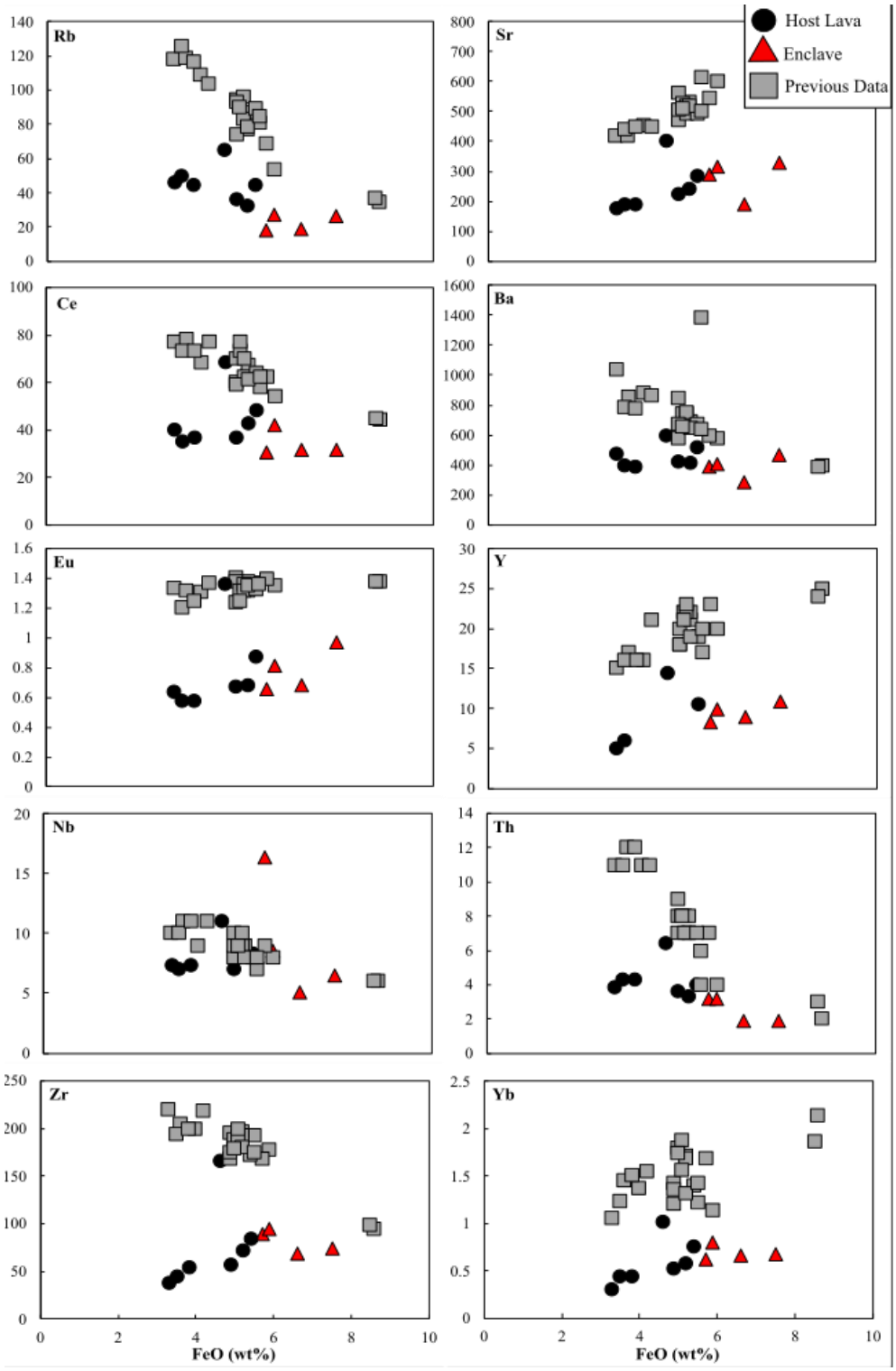

Figure 3: Whole rock trace element concentrations (parts per million; ppm) plotted against FeO wt% contents in comparison to previous data presented in Feeley & Davidson, (1994).

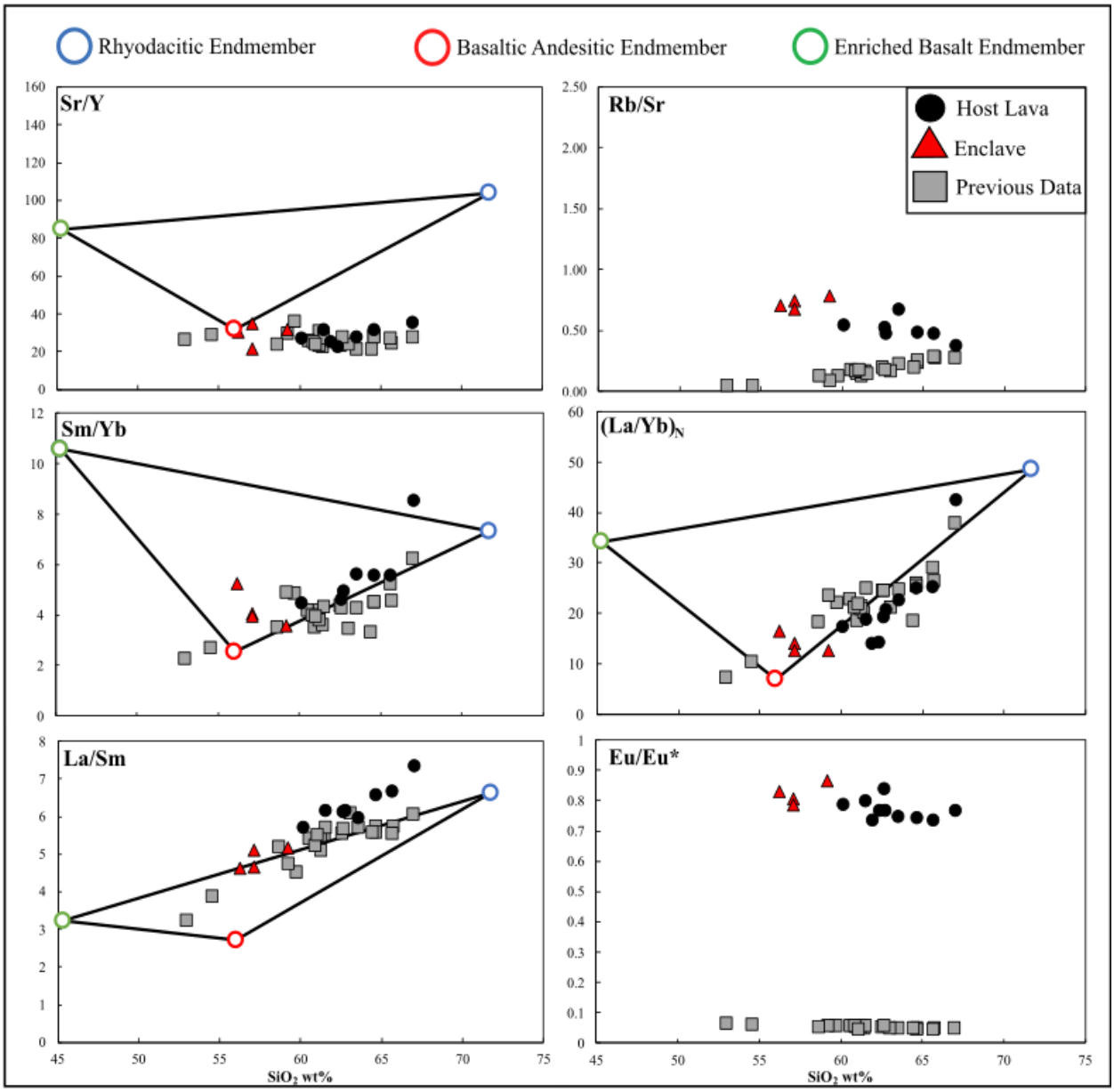

Figure 4: Selected trace element ratios of whole rock samples with corresponding major element data from Feeley & Davidson, (1994).

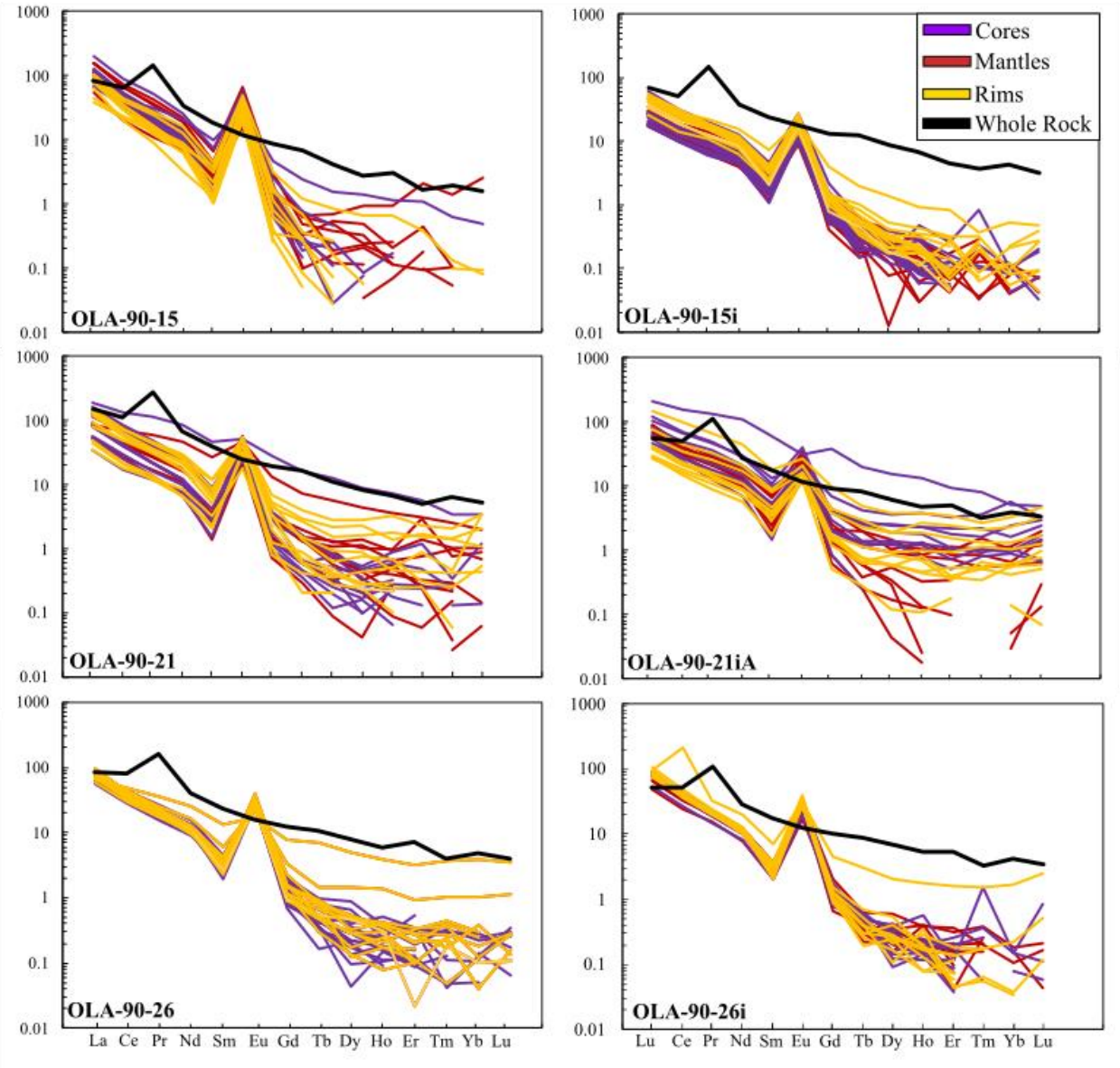

Figure 5: Chondrite normalized trace element concentrations for plagioclase feldspar phenocrysts subjected to LA-ICP-MS analysis in comparison to their respective whole rock values. Chondrite values used for normalization are derived from McDonough & Sun, (1995). Increasing y-axis indicates increasing enrichment of elements relative to chondrite.

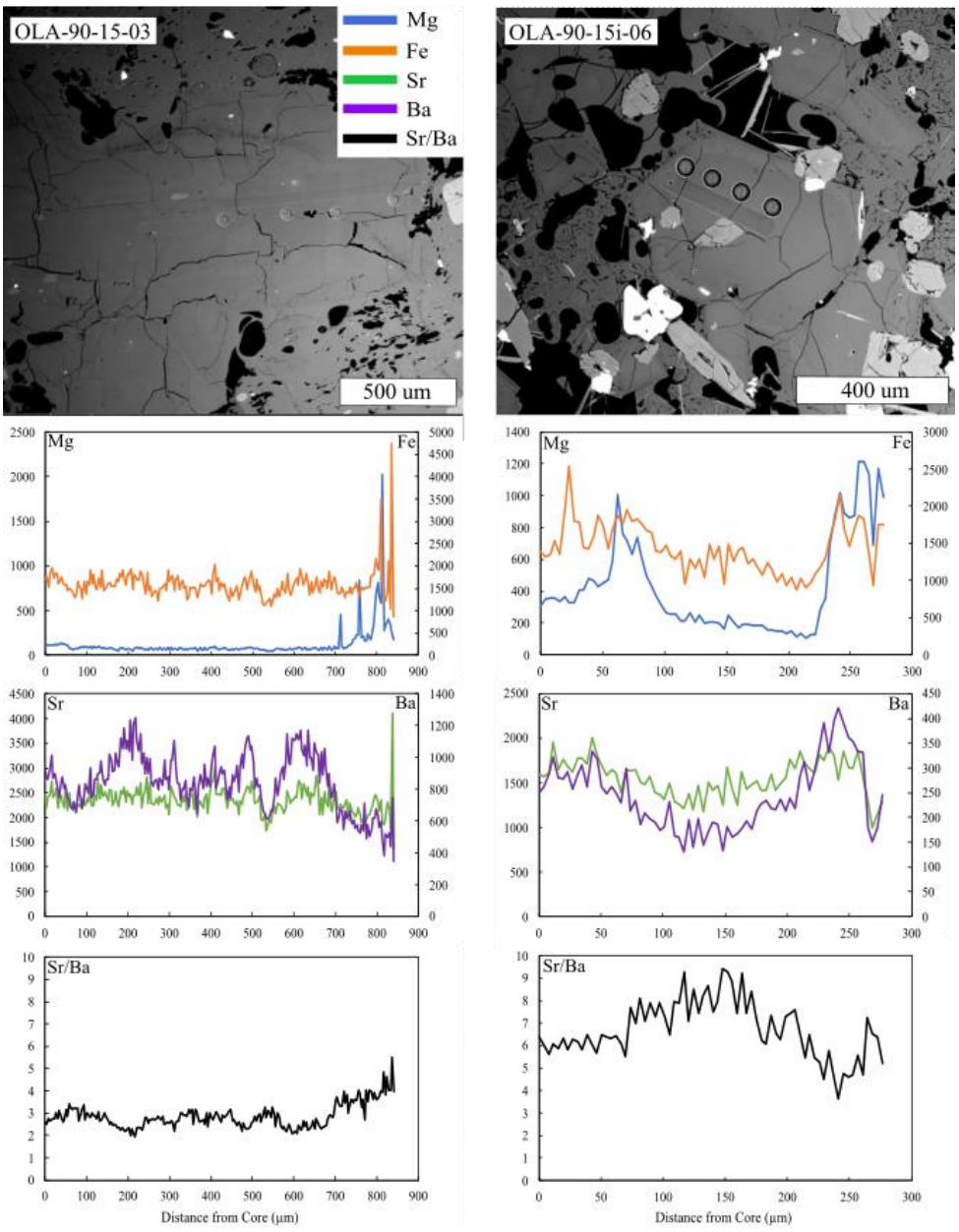

Figure 6: Backscatter electron (BSE) imagery representative of plagioclase feldspar phenocrysts in host lava sample OLA-90-15 and corresponding magmatic enclave sample OLA-90-15i. Transects beneath BSE images are from core-to-rim transect analyses of the pheoncrysts. Y-axis units are in parts per million (ppm).

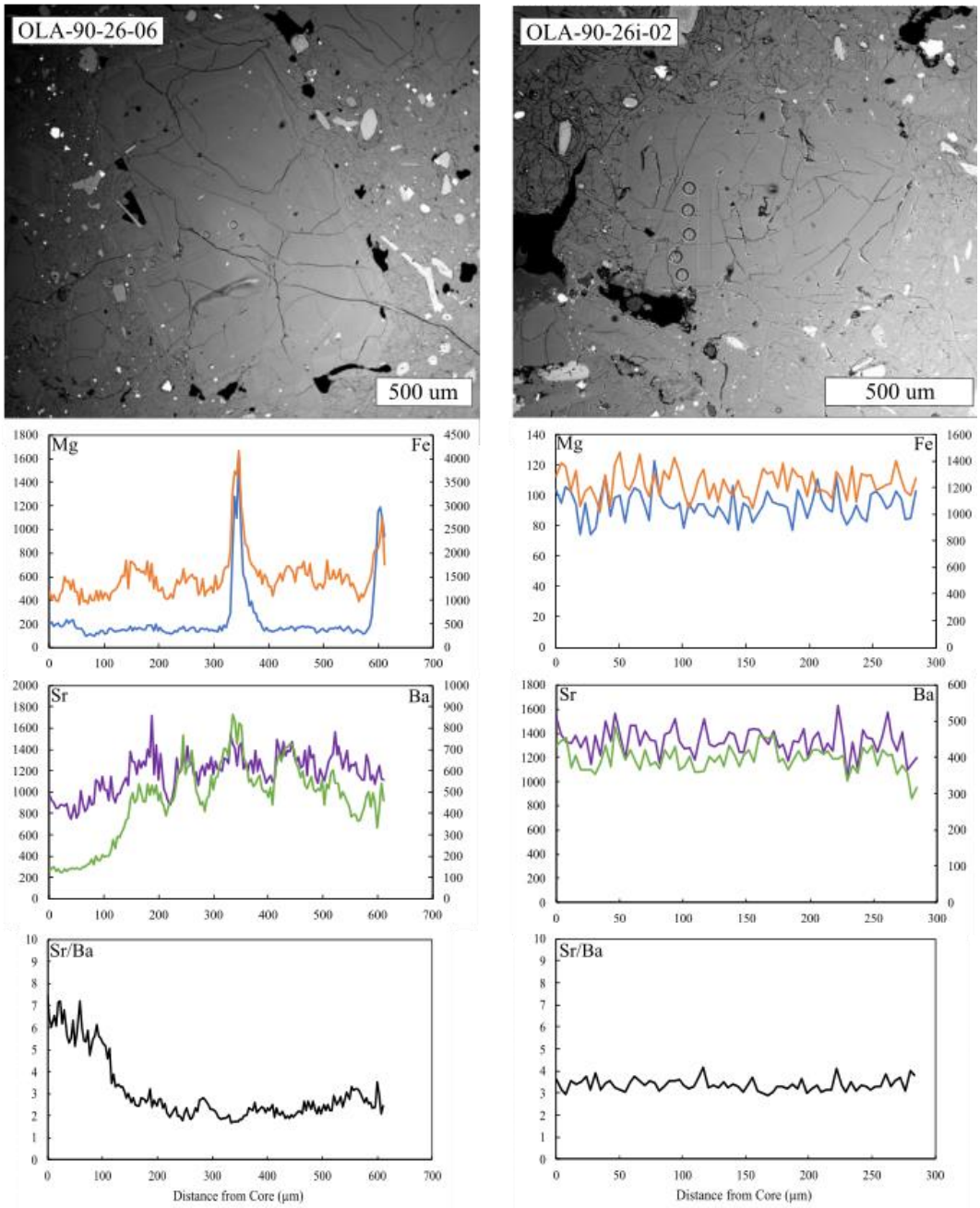

Figure 7: Backscatter electron (BSE) imagery representative of plagioclase feldspar phenocrysts in host lava sample OLA-90-21 and corresponding magmatic enclave sample OLA-90-21iA. Transects beneath BSE images are from core-to-rim transect analyses of the pheoncrysts. Legend is identical to that of Figure 6. Y-axis units are in parts per million (ppm).

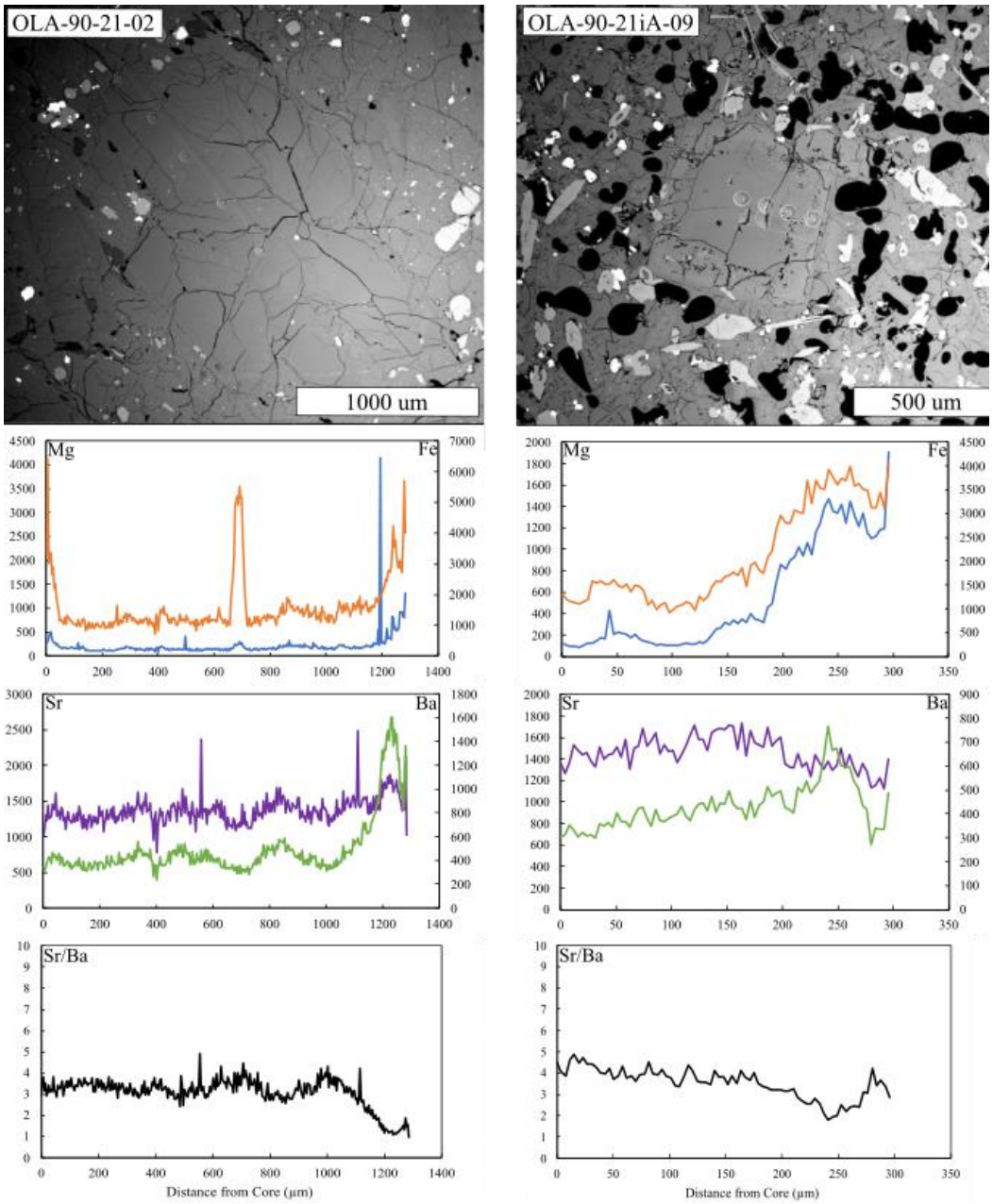

Figure 8: Backscatter electron (BSE) imagery representative of plagioclase feldspar phenocrysts in host lava sample OLA-90-21 and corresponding magmatic enclave sample OLA-90-21iA. Transects beneath BSE images are from core-to-rim transect analyses of the pheoncrysts. Legend is identical to that of Figure 6. Y-axis units are in parts per million (ppm).

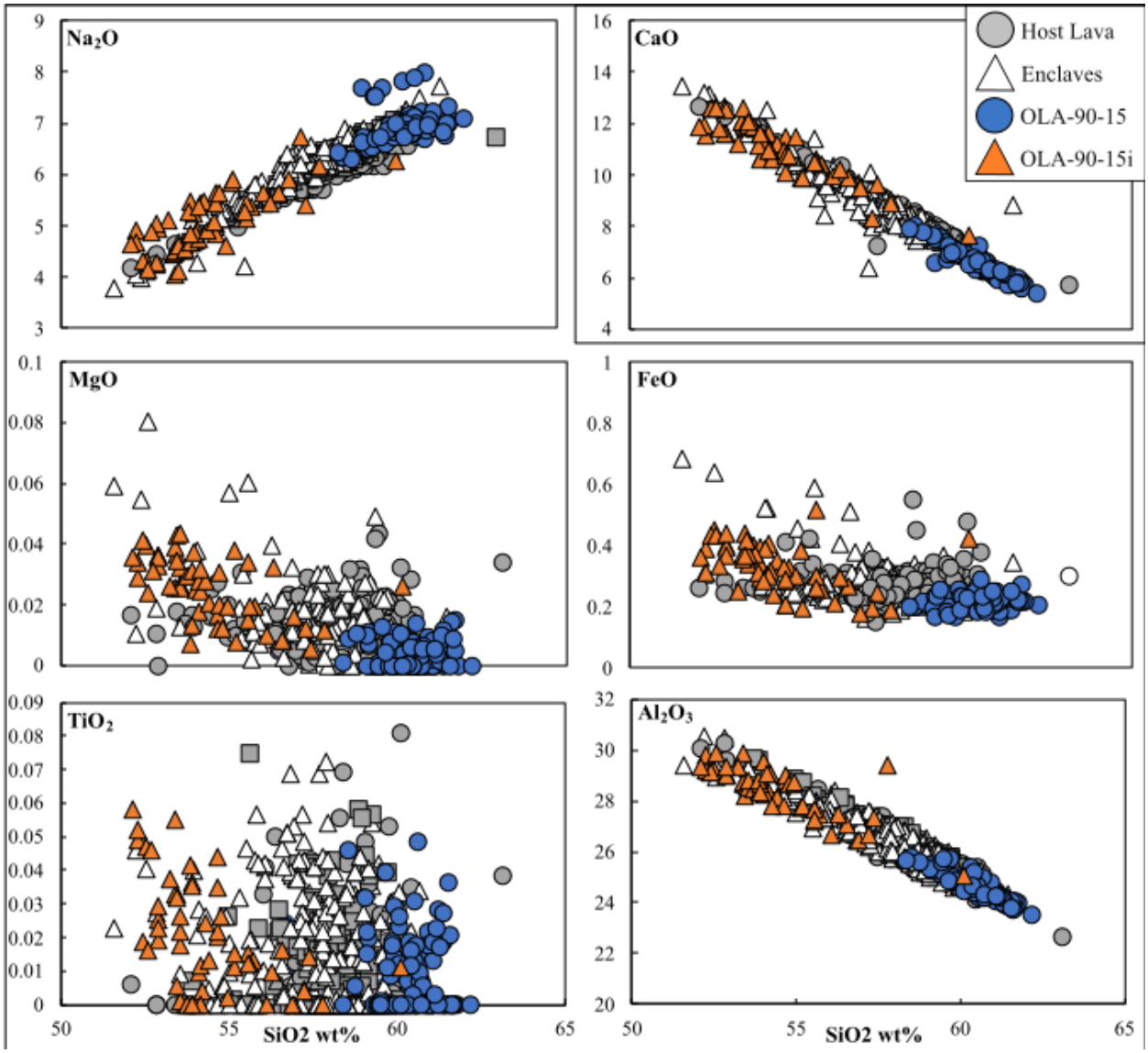

Figure 9: Plagioclase major element weight percentages (wt%) plotted against SiO_2 wt% contents. Plagioclase feldspar from host lava sample OLA-90-15 and corresponding magmatic enclave sample OLA-90-15i have been highlighed to denote the relative disparity.

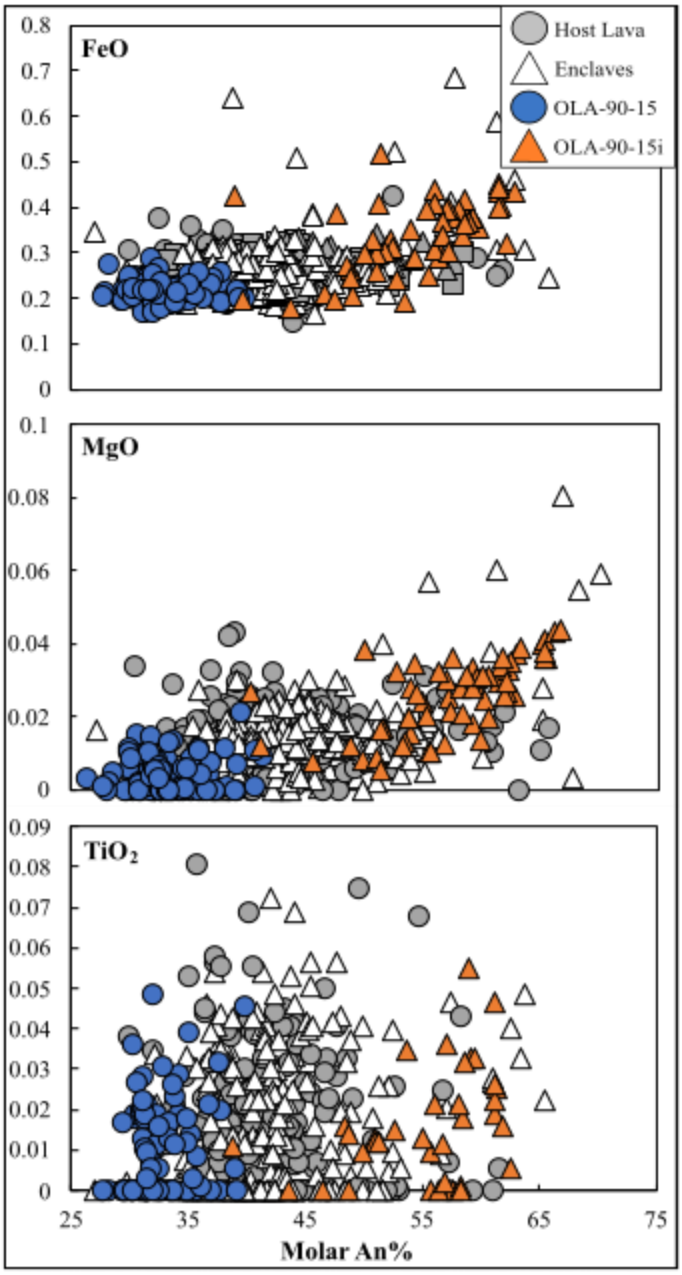

Figure 10: FeO, MgO, and TiO_2 wt% contents plotted against molar An contents. Points originatng from host lava sample OLA-90-15 and correspsonding enclave sample OLA-90-15i are highlighted.

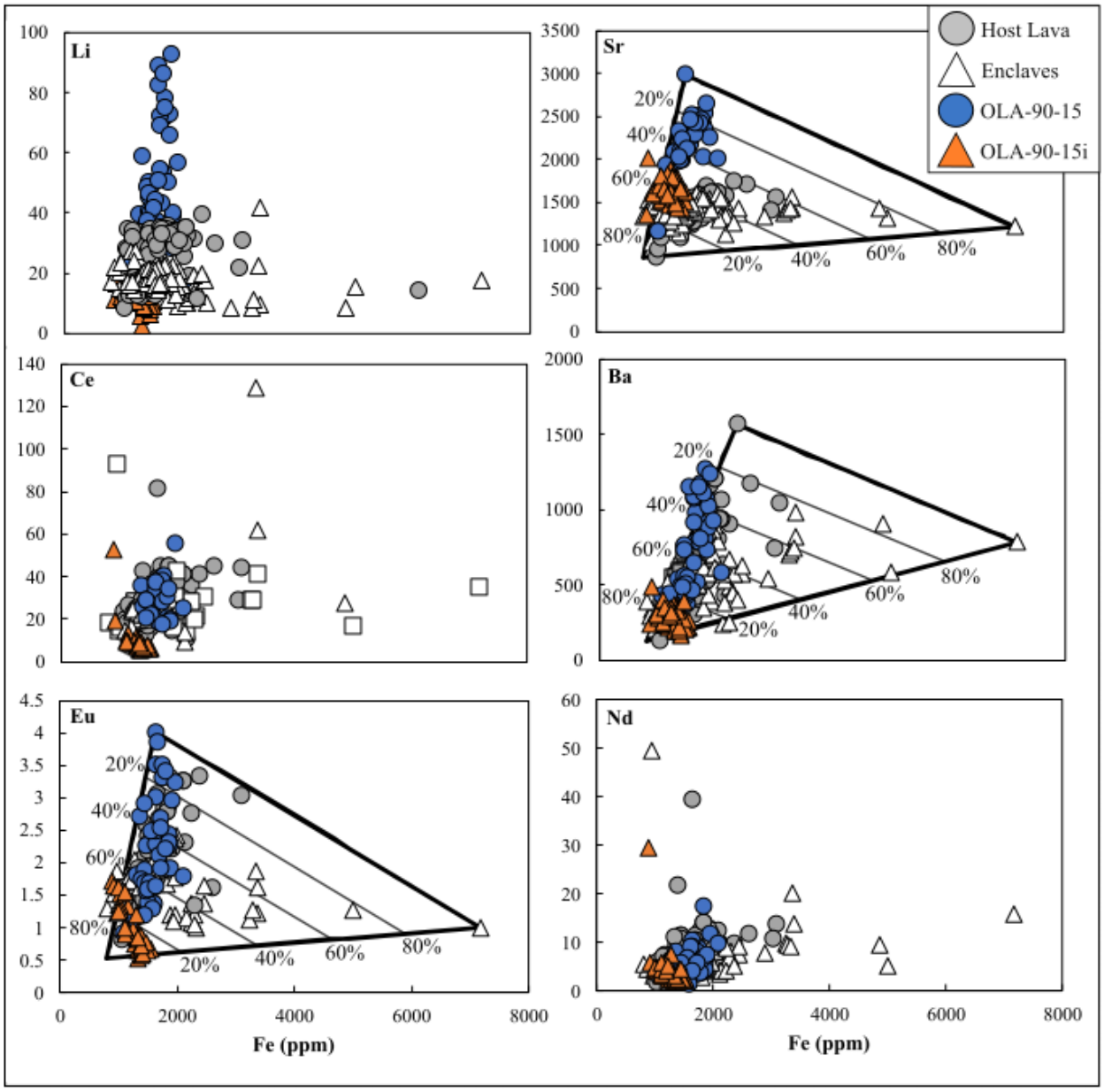

Figure 11: Plagioclase feldspar trace element concentrations (ppm) plotted against Fe concentrations. Mixing lines between element end-members (black lines) and minor mixing (grey lines) are imposed on select element plots. Points originating from host lava sample OLA-90-15 and correspsonding enclave sample OLA-90-15i are highlighted.

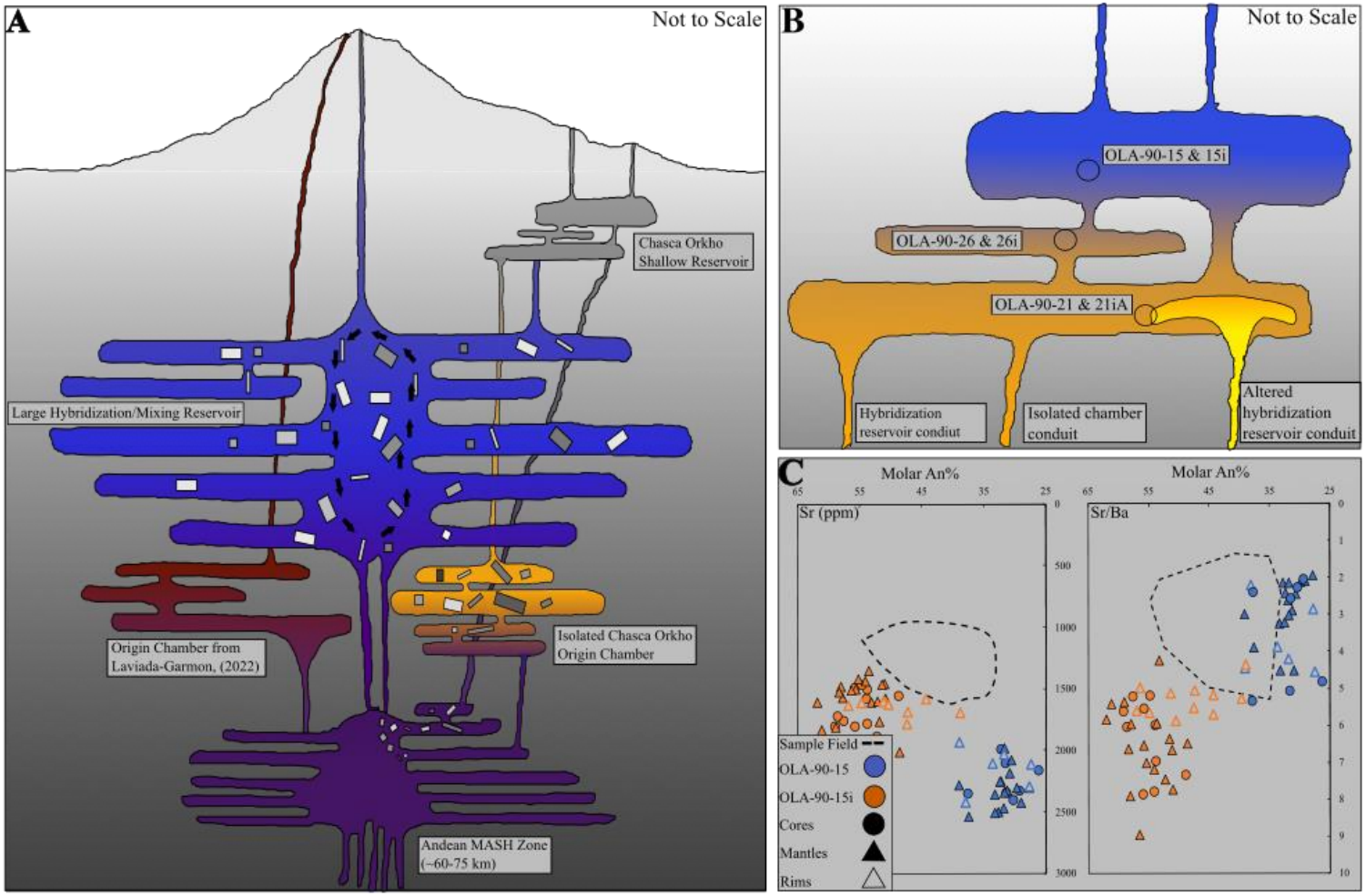

Figure 12: **(A)** Interpreted model of the magmatic system beneath Volcán Ollagüe at the time of the Chasca Orkho eruption. Plagioclase phenocrysts from our samples are inferred to originate from 1) an origin chamber unique to the eruption; 2) a large hybridization reservoir that periodically intruded into the shallow reservoir; and 3) the Andean MASH Zone . **(B)** Reconstruction of the Chasca Orkho shallow reservoir with theorized placement of magmas represented by samples utilized for this research. **(C)** Sr concentrations and Sr/Ba ratios plotted against molar An content depicting samples OLA-90-15 and OLA-90-15i in relation to the rest of the samples (field).